UNIVERSITAT POLITÈCNICA DE CATALUNYA
BARCELONATECH
Escola d'Enginyeria de Barcelona Est

FINAL MASTER PROJECT

Degree in Materials Engineering

BIOMATERIALS WITH ANTIMICROBIAL PROPERTIES FOR BONE REGENERATION

Report

Author: Camille LAFFERRANDERIE
Director: Maria Pau GINEBRA MOLINS
Co-Director: Montserrat ESPANOL PONS

Call: February 2019

Abstract

Calcium phosphates are widely used materials in bone regeneration due to their composition very close to the bone mineral phase. However despite their great success in bone regeneration, they can be seriously threatened if bacterial infection occurs. Since antimicrobial resistance makes antibiotics largely ineffective, other alternatives are required to fight infection. Recent studies have shown that the material topography can help preventing bacterial adhesion and even kill attached bacteria.

In this project, the adhesion and the proliferation of bacteria *Staphyloccocus aureus* are studied on four calcium phosphates with different topographies. These materials are developed in the first phase of the project. The coarse calcium deficient hydroxyapatite C-CDHA material has a surface made of microplate-like crystals whereas the fine calcium deficient hydroxyapatite F-CDHA is made of nanometric needle-like crystals. Moreover, the beta-tricalcium phosphate β-TCP, obtained at high temperature, presents a smooth topography of polyhedral grains. Finally, a compacted material Fc-CDHA, obtained from F-CDHA, is analyzed to study bacterial behavior on a perfectly smooth surface and serves as a control for the other materials. The second phase of the project is the study of bacterial adhesion and proliferation on the surface of these materials. Two approaches are conducted to asses the amount of bacteria. The first approach measures bacterial surface coverage through fluorescence imaging, while in the second approach bacteria are first detached and subsequently quantified in a spectrophotometer.

The results clearly showed that F-CDHA material, due to its nanometric topography, was the most suitable material reducing bacterial proliferation. Besides, the results on the quantification of *Staphyloccocus aureus* from the different surfaces were also very promising although a better detaching method needs to be developed to have more conclusive results.

Résumé

Depuis plusieurs décennies, les phosphates de calcium sont devenus les matériaux idéaux dans le secteur de la régénération osseuse en raison de leur composition très proche de celle de la phase minérale osseuse. Cependant, malgré leurs nombreux atouts, ils peuvent être menacés lors d'infections bactériennes. En effet, puisque la résistance antimicrobienne rend un grand nombre d'antibiotiques inefficaces, d'autres alternatives doivent être élaborées pour lutter contre les infections. De récentes études montrent que la topographie des matériaux peut aider à éviter l'adhésion bactérienne et même tuer les bactéries adhérées.

Au cours de ce projet, l'adhésion et la prolifération de bactéries *Staphyloccocus aureus* est étudiée sur plusieurs phosphates de calcium aux topographies radicalement différentes. L'élaboration de ces matériaux est présentée dans la première phase du projet. L'hydroxyapatite grossière carencée en calcium C-CDHA présente une surface couverte de cristaux composés de microplaques alors que l'hydroxyapatite fine carencée en calcium F-CDHA présente une topographie de cristaux composés d'aiguilles nanométriques. D'autre part, le beta phosphate tricalcique β-TCP, obtenu à haute température, présente une topographie lisse de cristaux polyhédraux. Enfin, un matériau compacté Fc-CDHA, fait à partir de F-CDHA, est analysé pour étudier le comportement bactérien sur une surface parfaitement lisse et sert également de contrôle pour l'étude des autres matériaux. La deuxième phase du projet est l'étude de tests d'adhésion et de prolifération bactérienne à la surface de ces matériaux. Deux approches sont menées: l'approche conventionnelle et qualitative permet la détermination du pourcentage d'aire occupée par les bactéries à la surface des matériaux et une approche quantitative basée sur le détachement des bactéries *Staphyloccocus aureus*.

Les résultats montrent clairement que le matériau F-CDHA semble être le matériau le plus propice pour réduire la prolifération bactérienne. D'autre part, les résultats de la quantification des bactéries sur les différentes surfaces sont également très prometteurs bien qu'une meilleure méthode de détachement nécessite d'être développée pour obtenir des résultats plus concluants.

Resumen

Los fosfatos de calcio se han convertido en materiales ideales para la regeneración ósea debido a su composición muy similar a la de la fase mineral ósea. Sin embargo, a pesar de su gran éxito en la regeneración ósea, pueden verse seriamente amenazados si se produce una infección bacteriana. Dado que la resistencia antimicrobiana hace que los antibióticos sean en gran medida ineficaces, se requieren otras alternativas para combatir las infecciones. Estudios recientes han demostrado que la topografía del material puede ayudar a prevenir la adhesión bacteriana e incluso matar las bacterias adheridas.

Durante este proyecto, se estudia la adhesión de las bacterias *Staphylococcus aureus* en varios fosfatos de calcio con topografías radicalmente diferentes. El desarrollo de estos materiales se presenta en la primera fase del proyecto. La hidroxiapatita gruesa deficiente en calcio, C-CDHA tiene una superficie recubierta de cristales compuestos por microplacas, mientras que la hidroxiapatita fina deficiente en calcio F-CDHA tiene una topografía de cristales compuestos por agujas nanométricas. Por otro lado, el beta fosfato tricálcico β-TCP, obtenido a alta temperatura, tiene una topografía suave con cristales poliédricos. Finalmente, se analiza un material compactado Fc-CDHA, hecho a partir de F-CDHA, para estudiar el comportamiento bacteriano en una superficie perfectamente lisa y también sirve como control para el estudio de los otros materiales. La segunda fase del proyecto es el estudio de las pruebas de adhesión y de proliferación bacterianas en la superficie de estos materiales. Se realizan dos enfoques: el enfoque convencional que es qualitativo determina el porcentaje de area occupada por las bacterias en las superficies y un enfoque quantitativo fundado sobre desenganchar las bacterias *Staphyloccocus aureus*.

Los resultados del enfoque qualitativo muestran que el material F-CDHA parece ser el material más adecuado para reducir la proliferación bacterianas. Por otra parte, los resultados de la quantificación de las bacterias sobre las diferentes superficies son también muy prometedores aunque una mejora técnica para desenganchar las bacterias debe ser desarrollada para obtener resultados más conclusivos.

Acknowledgements

First of all, I would like to thank the Professor Maria Pau Ginebra for giving me the opportunity to carry out this project as my final master project within the Biomaterials, Biomechanics and Tissue engineering reasearch group.
I would like to thank very sincerely Joanna Sadowska who, since the beginning of the project, has not stopped of training me, advising me and supporting me in the actions and reflections that I led and whose participation was essential for the good proceedings of this project.
I would like to extend my gratitude to the Professor Montserrat Espanol Pons who has always been available to meet me and discuss about the project progress and also for his reasonable and stimulating suggestions.
I would also like to thank Joaquim Minguela for showing me how to handle bacteria and the precautions that must be taken in bacterial experiments.
Finally, I thank my family as well as my relatives who encouraged me throughout this project.

Glossary

α-TCP: Tricalcium phosphate alpha form

β-TCP: Tricalcium phosphate beta form

BHI: Brain heart infusion

CaP: Calcium phosphates

C-CDHA: Coarse calcium deficient hydroxyapatite

CDHA: Calcium deficient hydroxyapatite

CFU: Colony Forming Units

CPCs: Calcium phosphate cements

HA: Hydroxyapatite

Fc-CDHA: Fine compacted calcium deficient hydroxyapatite

F-CDHA: Fine calcium deficient hydroxyapatite

L/D: Live/Dead staining

PBS: Phosphate buffered saline

SA: *Staphylococcus aureus*

SEM: Scanning electron microscope

TCP: Tricalcium phosphate

XRD: X-ray diffraction

Contents

1 Introduction

During a surgical procedure, the body is subject to many risks of infection. Very easily bacteria can adhere to the surface of implanted materials and contaminate the treated area. Faced with bacterial resistance to antibiotics, new infection prevention strategies are required. Calcium phosphates, which are materials widely used in bone regeneration because of their remarkable properties, are therefore also confronted with these new questions. It is in this context that the 6-month research project untitled "Biomaterials with antimicrobial properties for bone regeneration" was set at the Biomaterials, Biomechanics and Tissue engineering (BBT) laboratory of the Polytechnic University of Catalonia (UPC). The subject of the project focused on assessing the potential of calcium phosphates with different topographies on bacterial growth and to develop a method to better quantify the results. Indeed, the topography of a material plays a primordial role during the bacterial adhesion. According to many studies, some topographies, due to their size or regularity, can control, promote and even prevent bacterial adhesion and thus bacterial proliferation within the patient's body.

During this project, four calcium phosphate materials with different topographies are prepared, characterized and incubated with *Staphyloccocus aureus* bacteria. Regarding, cell adhesion and proliferation, two different assays are performed. Firstly, a qualitative assay based on the assessment of the percentage of bacterial surface coverage by Live/Dead staining of the samples. Secondly, a quantitative method based on the bacterial detachment from the samples followed by quantification in a spectrophotometer. It is expected that the understanding of bacterial adhesion and proliferation on the four topographically different calcium phosphates will help in the design of better bone substitutes with improved antimicrobial properties.

1.1 Objectives

- To determine the potential for *Staphylococcus aureus* adhesion and proliferation on four topographically different calcium phosphate (CaP) materials:
  - C-CDHA: Precipitated CaP made of plate-like crystals at 37°C.
  - F-CDHA: Precipitated CaP made of needle-like crystals at 37°C.
  - β-TCP: Sintered CaP made of polyhedral grains at 1100°C.
  - Fc-CDHA: Control CaP with flat surface.
- To quantify bacterial adhesion comparing two methods:
  - The conventional approach which quantify bacterial surface coverage by fluorescent labeling.
  - An adapted approach based on the detachment of bacteria and following their growth.

2 State of the art

Upon damage of the structure of bone due to fracture or tumour resection, biomaterials are needed to fix and to assist its regeneration. Metals, polymers and ceramics are nowadays the main materials employed as implants in traumatology. Moreover, in many researches, it has been demonstrated that calcium phosphate biomaterials (CaPs) such as hydroxyapatite or tricalcium phosphate have a remarkable potential due to their unique properties in terms of their composition. In fact, the inorganic phase of bone tissues is made of calcium phosphate.

However, when an implant is inserted in the body of a patient, there is still a fairly significant risk of developing either a fungal or bacterial infection. Similarly, there is also the risk of a serious inflammatory process occurring around the implant and leading to their rejection. That is why many sanitary precautions are taken by surgeons and nurses during surgery. They work for instance in a sterile atmosphere and with sterilized equipments. Nevertheless, the zero risk scenario does not exist and infection can despite everything still occur. The most common way to fight bacterial or microbial infections is through the prescription of antibiotics to the patient. Unfortunately, due to the misuse of antibiotics many bacteria have become resistant to them. Therefore, antibiotics do not appear anymore as an infallible solution and alternative solutions are required to prevent implant infections.

2.1 Calcium phosphates in bone regeneration

2.1.1 Bone mineralization

2.1.1.1 Bone structure

Bones are organized at several levels as shown in Figure 1 from the macro all the way to the nanoscale. Bone is composed by two parts, an organic one composed by microfibrils of collagen and an inorganic one composed of hydroxyapatite crystals [1]. These parts are organized hierarchially. In fact, during the bone formation, the collagen is firstly laid down and after the apatite mineralization occurs. It has been determined that apatite crystallites nucleate and grow in the collagen network into two different sizes. The apatite crystallites can grow in the holes between terminations of end-to-end-aligned collagen microfibrils but also in smaller pores between side-by-side collagen microfibrils. The main cells responsible for the mineralization are the osteoblastic cells which release calcium and phosphate into the body fluids and consequently generate bone matrix. On the other hand, the osteoclastic cells intervene during the bone turnover cycle and they dissolve the old bone by releasing hydrolytic enzymes and protons [2].

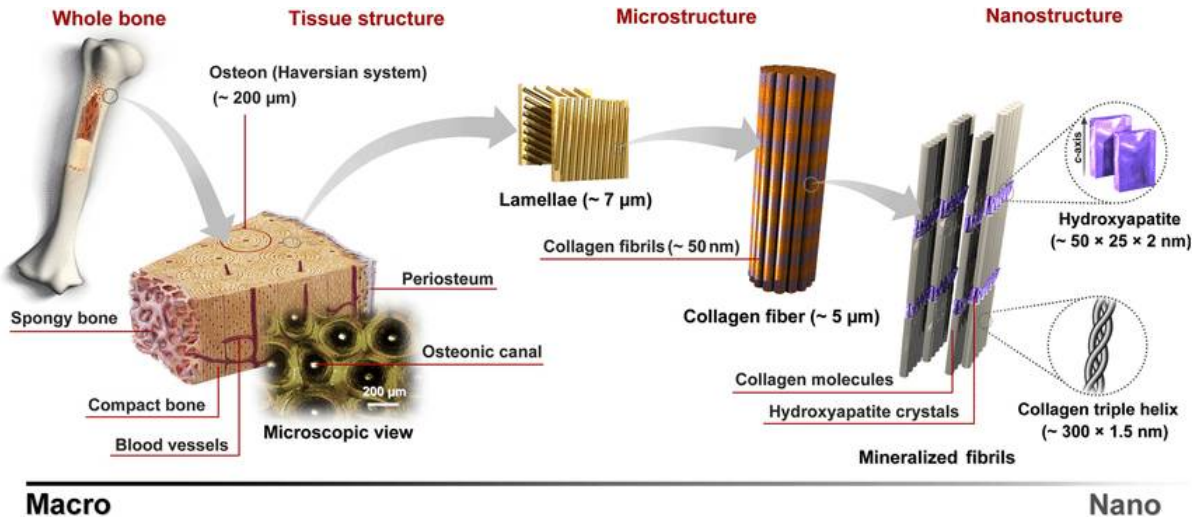

Figure 1: Hierarchical structure of a typical bone. Presentation of the tissue structure, the microstructure, and the nanostructure [3].

2.1.1.2 Bone composition

The proportion of organic and inorganic phase in bone depends on the type of biomineralized material (bones or teeth) and concerning bones, the composition is approximately 45-70 wt% of mineral, 10 wt% of water and the rest is collagen and a small quantity of non collagenous proteins [2]. Many researches have identified that the main mineral component of bones is a biologically produced analogue of hydroxyapatite $Ca_5(PO_4)_3OH$. However, bioapatites present a lower calcium/phosphate atomic ratio than the stoichiometric hydroxyapatite value of 1,67. In fact, natural bones are made up of a carbonated calcium deficient hydroxyapatite [2][4].

2.1.2 Calcium phosphates

Calcium phosphate (CaP) compounds are becoming increasingly important in the field of biomaterials and, in particular, as bone substitutes. With the exception of calcium pyrophosphate ($Ca_2P_2O_7$), most calcium phosphates previously used *in vivo* have been the calcium orthophosphates (CaP) which contain the orthophosphate group $(PO_4)_{3-}$ [5].
A list of the main calcium phosphates are presented in Table 1. They are classified according to their Ca/P molar ratio.
The Ca/P molar ratio is an indicator of the calcium phosphate acidity and solubility. In fact, the lower the ratio is, the more acidic and soluble the CaP become. The property of solubility is key in the design of biomaterials for bone regeneration. In fact, the solubility of a biomaterial has to be close or slightly below the solubility of the bone mineral phase to support bone growth. If the calcium phosphate is less soluble than the inorganic phase, its degradation will be slow despite the aid of osteoclasts. On the contrary, if the calcium phosphate is too soluble, it will be degraded before bone regeneration can take place.

Ca/P molar ratio	Compound	Formula
0.5	Monocalcium phosphate monohydrate (MCPM)	$Ca(H_2PO_4)_2 \cdot H_2O$
0.5	Monocalcium phosphate anhydrous (MCPA)	$Ca(H_2PO_4)_2$
1.0	Dicalcium phosphate dihydrate (DCPD), mineral brushite	$CaHPO_4 \cdot 2H_2O$
1.0	Dicalcium phosphate anhydrous (DCPA), mineral monetite	$CaHPO_4$
1.33	Octacalcium phosphate (OCP)	$Ca_8(HPO_4)_2(PO_4)_4 \cdot 5H_2O$
1.5	α-Tricalcium phosphate (α-TCP)	$\alpha\text{-}Ca_3(PO_4)_2$
1.5	β-Tricalcium phosphate (β-TCP)	$\beta\text{-}Ca_3(PO_4)_2$
1.2–2.2	Amorphous calcium phosphate (ACP)	$Ca_xH_y(PO_4)_z \cdot nH_2O$, $n = 3–4.5$; 15–20% H_2O
1.5–1.67	Calcium-deficient hydroxyapatite (CDHA)[e]	$Ca_{10-x}(HPO_4)_x(PO_4)_{6-x}(OH)_{2-x}$[f] $(0 < x < 1)$
1.67	Hydroxyapatite (HA or OHAp)	$Ca_{10}(PO_4)_6(OH)_2$
1.67	Fluorapatite (FA or FAp)	$Ca_{10}(PO_4)_6F_2$
2.0	Tetracalcium phosphate (TTCP or TetCP), mineral hilgenstockite	$Ca_4(PO_4)_2O$

Table 1: List of the main calcium phosphates according to the Ca/P molar ratio [6]

The solubility isotherms of several CaP in water are presented in Figure 2. The solubility is expressed as the total amount of calcium ions in solution. When the solubility is too high, as for the MCPM for example, the biomaterial cannot be used alone as bone substitute [6].

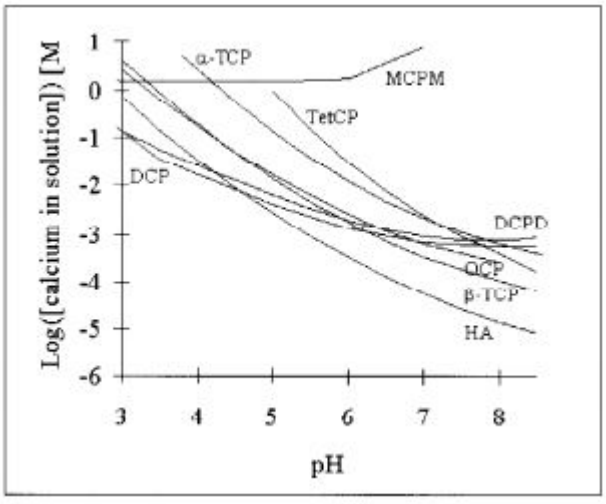

Figure 2: Solubility isotherms of several CaP in water. The solubility is expressed as the total amount of calcium ions in solution [7].

Two different categories of CaP can be distinguished: the CaP obtained by precipitation from an aqueous solution at or around room temperature called low temperature CaP and the CaP obtained by a thermal reaction, the high-temperature CaP. Table 2 gathers the main calcium phosphate in these two categories [5].

High temperature CaP	Low temperature CaP
α-tricalcium phosphate (α-TCP)	Dicalcium phosphate (DCP)
β-tricalcium phosphate (β -TCP)	Dicalcium phosphate dihydrate (DCPD)
Biphasic calcium phosphate (BCP)	Octocalcium phosphate (OCP)
Hydroxyapatite (HA)	Precipitated hydroxyapatite (PHA)
Monocalcium phosphate (MCP)	
Oxyapatite	
Tetracalcium phosphate (TetCP)	

Table 2: Classification of several calcium phosphates in two categories : high temperature and low temperature.

These differences in the processing temperature influence the materials' microstructure. In fact, at high temperature, ions are able to intensely diffuse and the grains grow in large polyhedral grains. On the other hand, at low temperature, aqueous precipitation leads to the formation of nanometric and micrometric crystals with composition and properties closer to the ones of bone. Among CaPs, tricalcium phosphate and hydroxyapatite are greatly used in bone regeneration.

2.1.2.1 Tricalcium phosphates

α-tricalcium phosphate (α-TCP, α-$Ca_3(PO_4)_2$) is nowadays an essential raw material in various medical applications such as injectable hydraulic bone cements, biodegradable bioceramics and composites for bone repair. As presented previously, they belong to the high-temperature CaP category.

It is known that there exist three polymorphs with the composition $Ca_3(PO_4)_2$: α-TCP, α'-TCP and β-TCP [8]. Nevertheless, several distinct phase equilibrium diagrams of the $CaO - P_2O_5$ system exist in the literature. They can be differentiated by the phase relationships. For instance, the transition temperatures of the phases can vary from a study to another. Figure 3 shows the phase equilibrium diagram determined by Kreidler and Hummel [9].

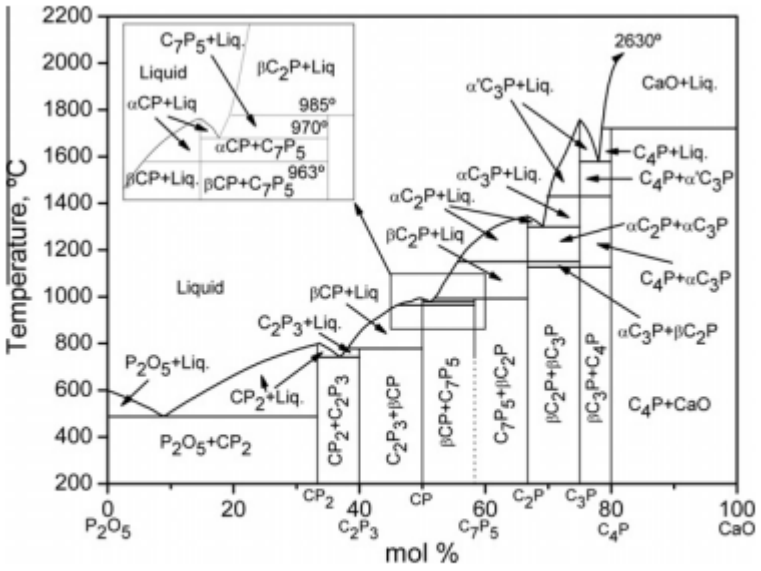

Figure 3: Phase equilibrium diagramm of $CaO - P_2O_5$ system [9]

As presented in Figure 3 the α'-$Ca_3(PO_4)_2$ phase, is observed above 1430°C until 2050°C or 2083°C according to different studies [10-14]. The α-$Ca_3(PO_4)_2$ in the absence of impurities is stable between 1120°C and 1470°C. The β-$Ca_3(PO_4)_2$ in its pure state is the phase stable below 1120°C. It has been noticed that the inclusion of small cations as impurities can stabilized the β-$Ca_3(PO_4)_2$ structure to temperatures above 1350°C. Finally, in a system free of moisture, it is stable at low temperature until near the room temperature [15]. On one hand, the transition from the α'-TCP to the α-TCP occurs between 1703°C and 1756°C [10][11][16]. On the other hand, the transition from the α-TCP to the β-TCP occurs between 1398°C and 1423°C [10][12][13].

Thus, α-TCP and α' TCP are formed at higher temperatures compared to the β-TCP. In fact, the α' form only exists at temperatures superior at 1430°C and reverts almost immediately to the α form on cooling below the transition temperature. On the contrary, the β-TCP is stable at room temperature and returns to the α form if it is heated at 1125°C and then is subjected to a quenching to room temperature. Due to the difficulty to be obtained, the α'-TCP does not represent a practical interest for biomedical applications.

In the α-TCP structure, the calcium and phosphate ions are packed in two kinds of columns along [001], one containing only cations and the other both cations and anions. A major difference with β-$Ca_3(PO_4)_2$ is that there are no cation-cation columns in the β form. Although both structures contain vacancies, the vacancies differ in type. Besides, α'-TCP consists of C-C and C-A columns alternating similarly to α-TCP [15][17].

The structure of α-TCP is less densely packed than β-TCP, and more densely than α'-TCP, as shown by the volumes per formula unit (V0) and the calculated theoretical density presented in Figure 4.

Property	$Ca_3(PO_4)_2$ polymorph		
	β-$Ca_3(PO_4)_2$ [30]	α-$Ca_3(PO_4)_2$ [28]	α'-$Ca_3(PO_4)_2$ [28]
Symmetry	Rhombohedral	Monoclinic	Hexagonal
V_0 (nm^3)	0.1680(2)	0.180(6)	0.19052(8)
D_{th} ($g\ cm^{-3}$)	3.066	2.866	2.702

Figure 4: Structural data of the $Ca_3(PO_4)_2$ polymorphs [8].

Despite their identical chemical composition, α-TCP and β-TCP differ in their structure, density and solubility. They are therefore used in different applications due to their distinct biological properties. For example, α-TCP is more soluble and hydrolyses forming calcium deficient hydroxyapatite that's why it is mainly employed as self-setting osteotranductive cements as a fine powder. We can also find α-TCP in the form of bioceramic granules and blocks. Usually, it is β-TCP which is used for preparing biodegradable bioceramics and ceramics as dense and macro-porous granules and blocks [8].

2.1.2.2 Calcium phosphate cements

The calcium phosphate cements (CPC) are biomaterials obtained by mixing one or more solid calcium phosphate salts with an aqueous solution forming a paste that has the ability to set (harden) with time. Typically, CaP cementation reactions take place at room temperature. The mechanism of cement setting reaction presented below is a dissolution precipitation process. During this reaction, a gradual hardening of the cement paste is observed. It is due to the entanglement of the precipitated crystals [5][18].

$$3Ca_3(PO_4)_2 + H_2O \longrightarrow Ca_9(HPO_4)(PO_4)_5OH$$

The different stages of the processing of calcium phosphate cements are illustrated in Figure 5. The microstructure is also described. As, the powder is mixed at low temperature with an aqueous solution, the dissolution of the particles occurs. The dissolved ions become supersaturated triggering the precipitation of $Ca_9(HPO_4)(PO_4)_5OH$ (CDHA) on the surface of α-TCP (α-$3Ca_3(PO_4)_2$). The final microstructure is made of aggregates of crystals entangled together. The material is very porous due to the voids in between crystals and in between crystal aggregates (Figure 5).

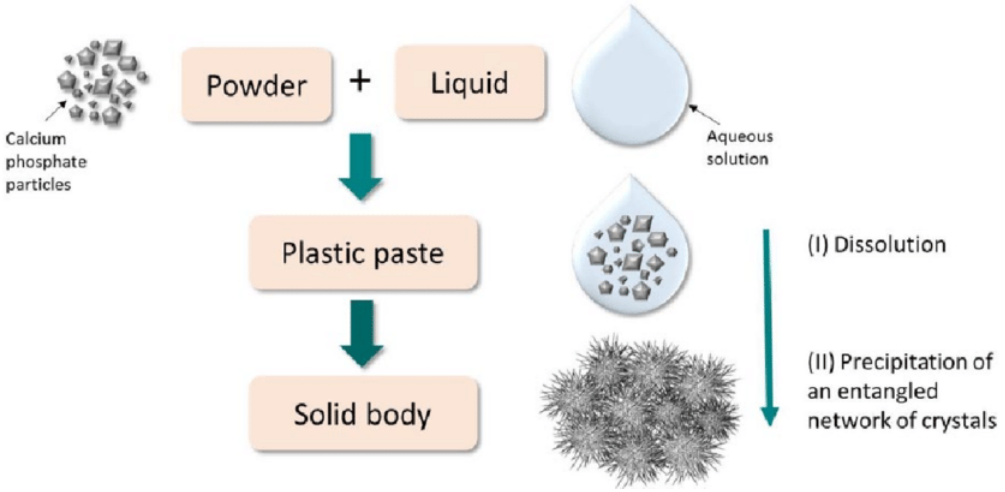

Figure 5: Processing of the calcium phosphate cements and microstructure evolution [4].

The possibility to inject calcium phosphate as pastes is to a great extent responsible for the CPCs success in the treatment of osteoporosis. Moreover, thank's to their remarkable biocompatibility, osteoconductivity and bioactivity, these materials, such as hydroxyapatite (HA) and calcium deficient hydroxyapatite (CDHA), are commonly used as bone tissue ingrowth support, drugs and bioactive molecules delivers [19][20].

2.2 Bacterial infection on implant surfaces

Despite their biocompatibility, CaP implants can be rejected by the patient's body. Their rejection is generally caused by bacterial infections which are the main cause of their failure.

2.2.1 Bacteria identification

Bacteria are biological cells belonging to the prokaryotic microorganisms. Prokaryotic microorganisms are single-celled microorganisms which have one free chromosome in their cytoplasm without a nuclear membrane [21]. Bacteria can be classified by several criteria such as their morphology. It exists three main shapes of bacteria: the bacili, the cocci and the spirilla. The bacilli are rod-shaped, the cocci are spherical and the spirilla have the shape of spirals. They are illustrated in Figure 6.

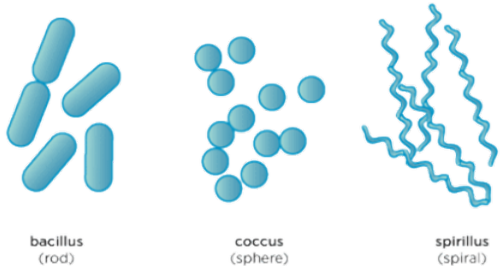

Figure 6: Common bacterial shapes: bacillus (rod), coccus (sphere) and spirillus (spiral) [22]

Furthermore, it is also interesting to characterise bacteria according to the structural characteristics of their cell wall. The principal goal of the cell wall is to protect the cytoplasm and acts as a barrier. It is composed by an inner layer, the cytoplasmic membrane whose goals are multiple. The cytoplasmic membrane is an osmotic barrier composed of enzymes and contributes to the regulation of the efflux of proteins responsible for antibiotic resistance. Moreover, a peptidoglycan layer ensures the shape of the bacteria and gives mechanical protection against osmotic pressure [22]. The thickness of the peptidoglycan layer varies depending on bacterial type. A method to differentiate a thin from a thick peptidoglycan layer was developed by the scientist Hans Christian Gram who gave his name as the Gram stain. The purpose of this technique is to separate most bacteria into two groups on the basis of the cell wall composition, gram-negative and gram-positive, by a differential staining. Figure 7 sketches the wall layers of the gram-negative and gram-positive bacteria.

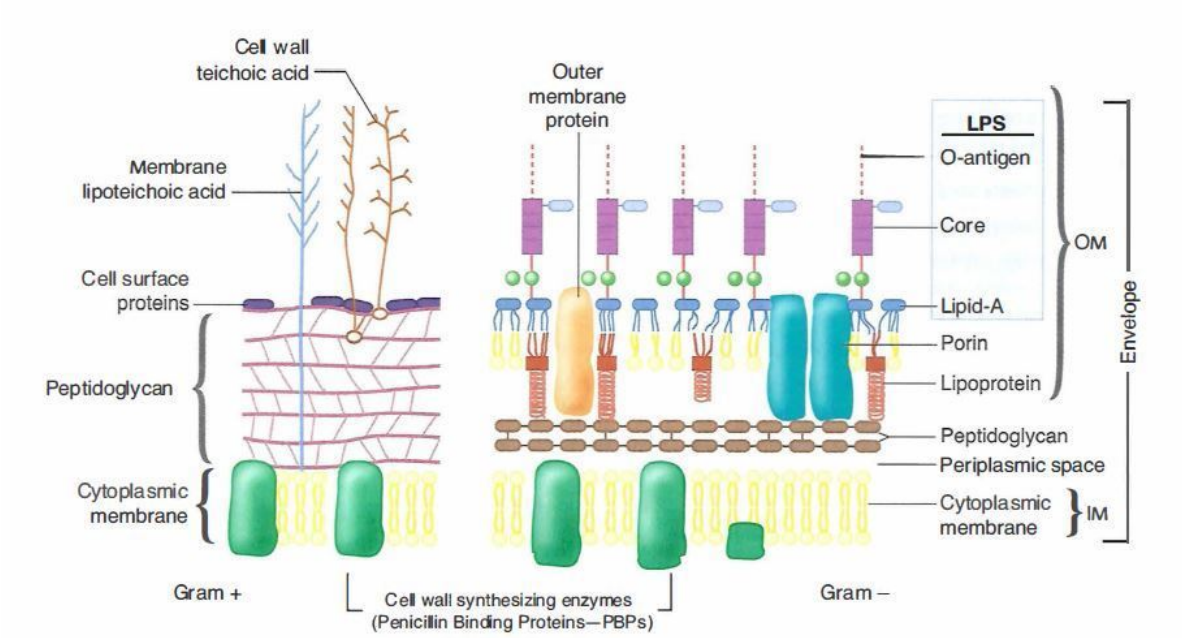

Figure 7: Description of the different layers of the bacteria wall of gram-positive bacteria (left) and gram-negative bacteria (right)[23]

The Gram stain method runs through several steps presented in Figure 8. The first step is to place bacteria on a microscope slide and to fix it by using a 90% solution of methanol and heating the slide with a flame. The methanol fixation preserves the morphology of the bacteria. Then, the microscope slide is submerged in a bath of gentian violet stain during few minutes. The gentian violet is fixed on the peptidoglycan layer and stains it in purple [24]. The stain stabilization is managed applying an iodine solution during 20 seconds. The iodine solution reacts with the gentian violet and forms a complex which keeps the bacteria purple. Afterward, the bleaching step is executed. The bleaching step distinguishes gram-negative from gram-positive bacteria. An organic solvent such ethanol or acetone is applied

to extract the dye from the peptidoglycan layer. Indeed, the solvent is able to dissolve the lipids contained in the outer membrane of the gram-negative bacteria, the lipopolysaccharide layer, exposing consequently the peptidoglycan layer and removing the purple stain. On the contrary, the peptidoglycan layer of the gram-positive bacteria is approximately 40 times thicker and highly cross-lined. It consequently avoids the bleaching. Thus, the gram-negative bacteria are colourless and the gram-positive remain purple. To reveal the gram-negative bacteria a counter stain, dye safranin, is added so they are finally stained in pink [25].

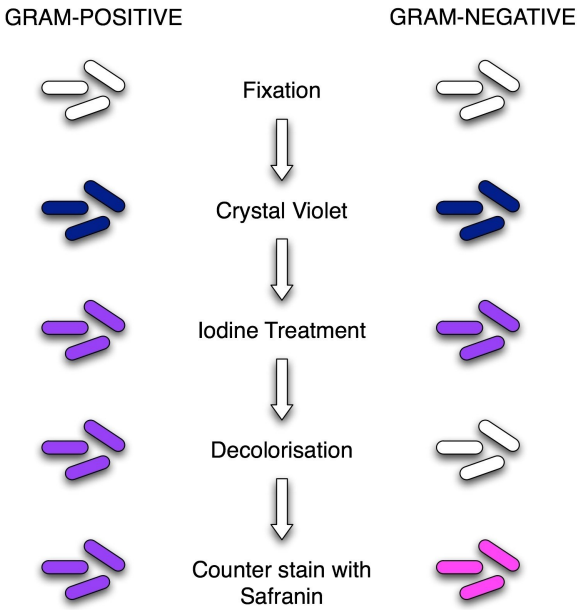

Figure 8: Gram stain identification steps [25]

Therefore, by combining morphology and Gram stain identification most bacteria can be classified as belonging to one of the four following categories: gram-negative cocci, gram-negative bacilli, gram-positive cocci and gram-positive bacilli. Hereinafter, an example of bacteria classifications combining morphology and gram stain identification is proposed in Figure 9 and indicates some bacteria species.

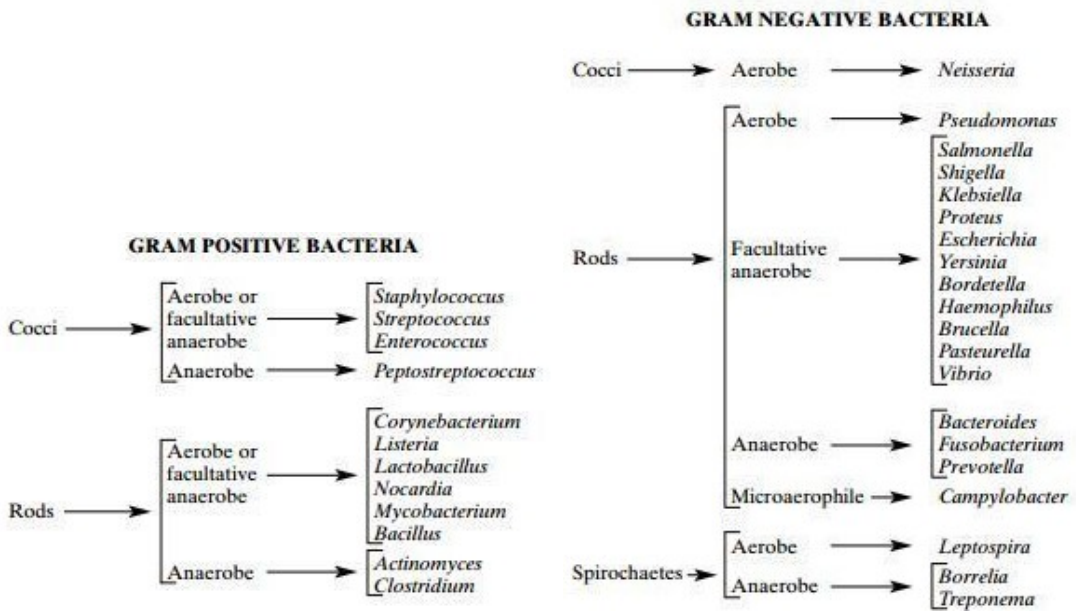

Figure 9: Bacteria classification by combining morphology and Gram staining [25]

The difference in composition and thickness that distinguishes the cell walls of gram positive and gram negative bacteria influences their respective properties. Indeed, the cell wall of gram negative bacteria is more susceptible to mechanical breakage. On the contrary, the thick layer of peptidoglycan offers high resistance to penetration and breakage to the gram positive bacteria.

However, due to the presence of the outer membrane made up of lipoproteins and other components, the cell of gram negative bacteria is not easily affected by antibodies or enzymes for instance [26].

2.2.2 Bacteria growth

Bacterial growth unfolds in four distinct stages. The first phase called lag phase starts when bacteria are added to the environment. During this phase, bacterial growth is slow as bacteria are acclimating to the nutrients and the new environment. The second phase is called the log or exponential phase because it is during this phase that bacteria are reproducing at their maximum rate. Moreover, the third phase is called the saturation or stationary phase. During this phase, the growth rate of the bacteria slows due to the depletion of nutrients and the accumulation of waste products. The fourth and final phase is called the death phase. In fact, it is at this point that bacteria begin to run out of nutrients and die [27].

These stages are presented in Figure 10.

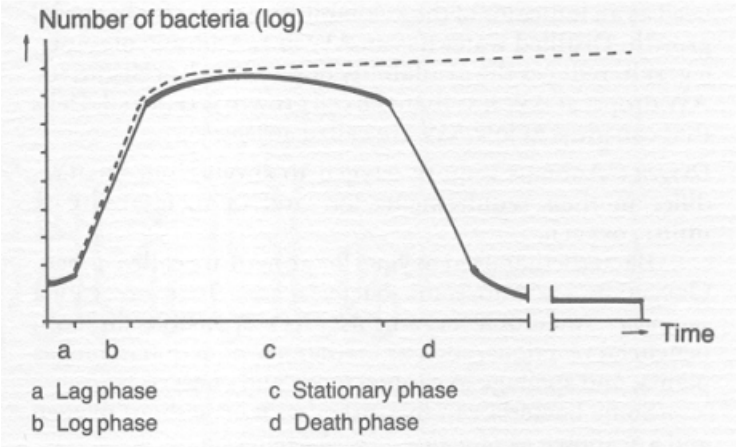

Figure 10: Stages of bacterial growth: lag phase (a), log phase (b), stationary phase (c) and death phase (d) [27]

2.2.3 Bacteria adhesion and biofilm formation

Bacteria present two types of growth mode, as a planktonic cell, i.e. floating as a simple cell, and as a sessile aggregate. They can attach to surfaces thanks to the presence of locomotor structures such as the flagella, proteins or polysaccharides. Once attached, the bacterium proliferates. The sessile mode of growth corresponds to the advanced growth mode of the planktonic cells [28]. Sessile aggregates also called biofilms constitute an association of bacteria stuck to each other in a matrix of extracellular polymeric substance produced by the bacteria themselves [29]. The extracellular polymeric substance is mainly composed of water at 97% and of other components as proteins, enzymes and polysaccharides. This environment allows a good transport of nutrients with the biofilm and also the elimination of the bacteria wastes. An example of biofilm chemical composition is presented in Table 3.

Components	Percentage of matrix
Microbial cells	2-5%
DNA and RNA	<1-2%
Polysaccharides	1-2%
Proteins	<1-2% (including enzymes)
Water	Up to 97%

Table 3: Example of biofilm composition [30]

The biofilm formation is a complex process that consists of several steps. It begins with the attachment of the bacteria to a surface then followed by the formation of micro-colonies, the three dimensional structure formation and ends with the detachment of the bacteria also called dispersal [30].

The different steps form a cycle and are illustrated in Figure 11.

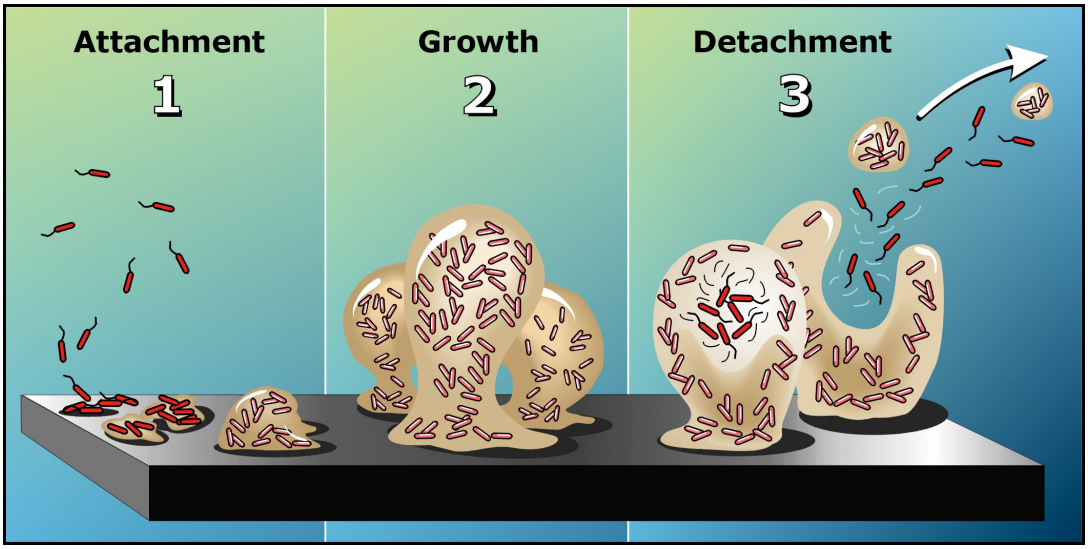

Figure 11: Biofilm formation steps [31]

The attachment of the bacteria is promoted if the surface is rough and hydrophilic. In addition, a solid-liquid interphase at 37°C is also a propitious environment for bacterial growth [30]. Once adhered, the multiplication of bacteria occurs and allows the micro-colonies formation. The biofilm is also in the adhesive bacterial behaviour. During micro-colony formation, exopolysaccharides are released to form a matrix with adhesins which are proteins on bacteria surface. This slimy matrix clearly intensifies bacterial adhesion [32]. A three dimensional structure is then elaborated. Channels filled of water appear and allow nutrients' transport and waste elimination within the biofilm. The last step of the biofilm life cycle is the dispersal of the bacteria. The secretion of specific enzymes produces the detachment of the planktonic bacteria from the biofilm. In addition, these bacteria keep the abilities developed in the biofilm such as the antibiotics resistance. Rapid multiplications and new biofilm formations are therefore generated [29]. Thus, biofilm formation represents a protected mode of growth that allows bacteria to survive in hostile environments, to resist to antibiotics and also to disperse and colonize new areas [33].

2.2.4 Antimicrobial resistance

Antibiotics are drugs used in bacterial infections treatments. Their purpose is to kill bacteria or to slow and avoid their growth.

Antimicrobial resistance (AMR) is recognized as one of the greatest threats to human health

worldwide. Just one organism, methicillin-resistant *Staphylococcus aureus* (MRSA), kills more Americans every year than emphysema, HIV/ AIDS, Parkinson's disease and homicides combined [34]. Data show a direct correlation between the use of antibiotics and the antimicrobial resistance. Countries with a higher consumption of antibiotics show higher rates of resistance [35]. Thus, the overuse of antibiotics puts patients at risks of adverse effects [36]. The resistance of *Staphylococcus aureus* to the antibiotics Oxacillin is illustrated in Figure 12. These data correspond to 2016.

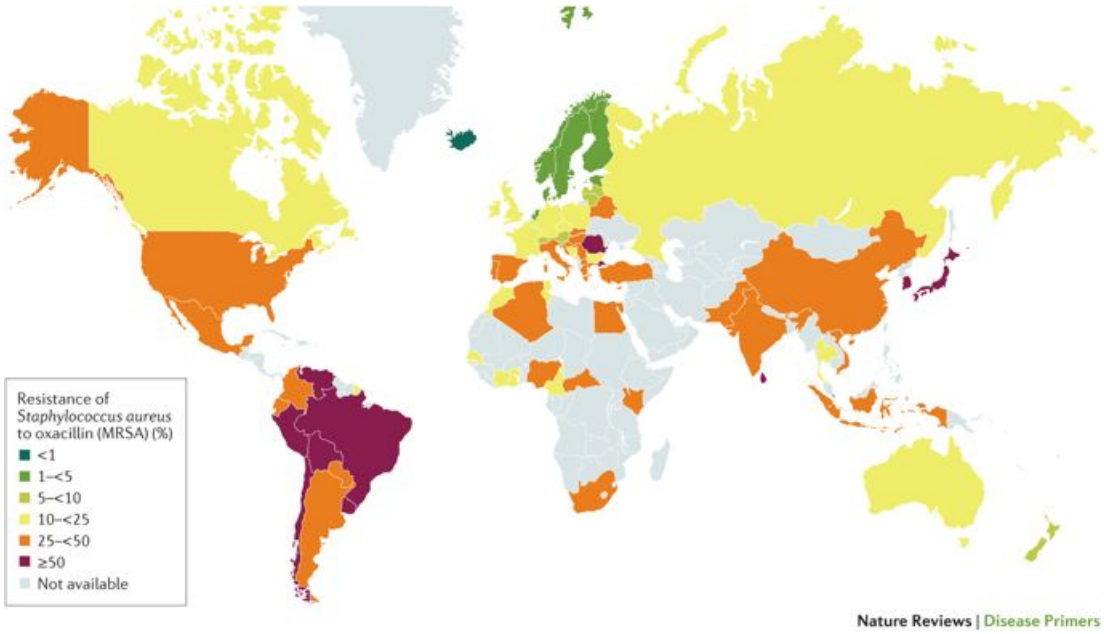

Figure 12: Resistance of *Staphylococcus aureus* to Oxacillin antibiotic all over the world in 2016 [37].

A reduction in antibiotics' consumption leads to a reduction of bacteria resistance. This explains the great interest in developing biomaterials which can avoid bacterial infection without antibiotics intervention.

2.2.5 Conventional treatments against bacterial infection

Bacterial adhesion and subsequent biofilm formation on biomedical implants and devices are the main cause of their failure. As therapeutic measures to control biomaterial-associated infections often fail and lead to severe consequences to the patient, emphasis has shifted to prevention of biomaterial-associated infections by designing antimicrobial biomaterials. The term "antimicrobial" can encompass different mechanisms of action such as antimicrobial-releasing strategies, contact killing or non-adhesivity. According to ISO 20743 antimicrobial activity refers to "the activity of an antibacterial finish used to prevent or mitigate the growth of bacteria, to reduce the number of bacteria or to kill bacteria" [38].

2.2.5.1 Antimicrobial releasing strategies

Antimicrobial coatings have become a very active field of research strongly stimulated by the increasing urgency of identifying alternatives of the traditional administration of antibiotics.

Released-based coatings exert their antimicrobial activity by leaching antibacterial compounds over time which allows killing both adhered and adjacent planktonic bacteria. It provides antibacterial activity only where it is needed, thus minimizing the development of resistance. The method to deliver these antibacterial compounds consists in coating surfaces by simple impregnation, by soaking a porous material or by coating with the desired antibacterial compounds [39].

A promising alternative to conventional antibiotics is the use of short cationic antimicrobial peptides (AMPs). These peptides are usually secreted by living organisms against pathogens. They are able to disrupt the membrane integrity or damage it by forming pores. They present an antimicrobial activity against both gram positive and gram negative bacteria [39].

A more recent approach to control the formation and the release of the antibacterial agents from coatings is to use polyelectrolyte multilayers (PEMs). In fact, PEMs are nanostructured polymeric systems and can be formed by layer-by-layer deposition, which consists on the growth of alternating layers with opposite charges. Antibacterial agent can either be trapped between layers or constitutes an integral part of the coating, by substituting one of the charged species.

An example of PEMs is presented in Figure 13. The multilayer film is based on polyarginine as polycation and hyaluronic acid as polyanion. The purpose of the polyarginine is to stimulate the macrophages proliferation and is later transformed in nitrite oxide which inhibits pathogens. Moreover, the hyaluronic acid which is a highly hydrated natural polysacharride is inhibitory to bacterial growth. In addition, it has shown angiogenic and anti-inflammatory properties [40]. The solution of silver has the role of reservoir and has a strong initial biocidal effect during the first few days.

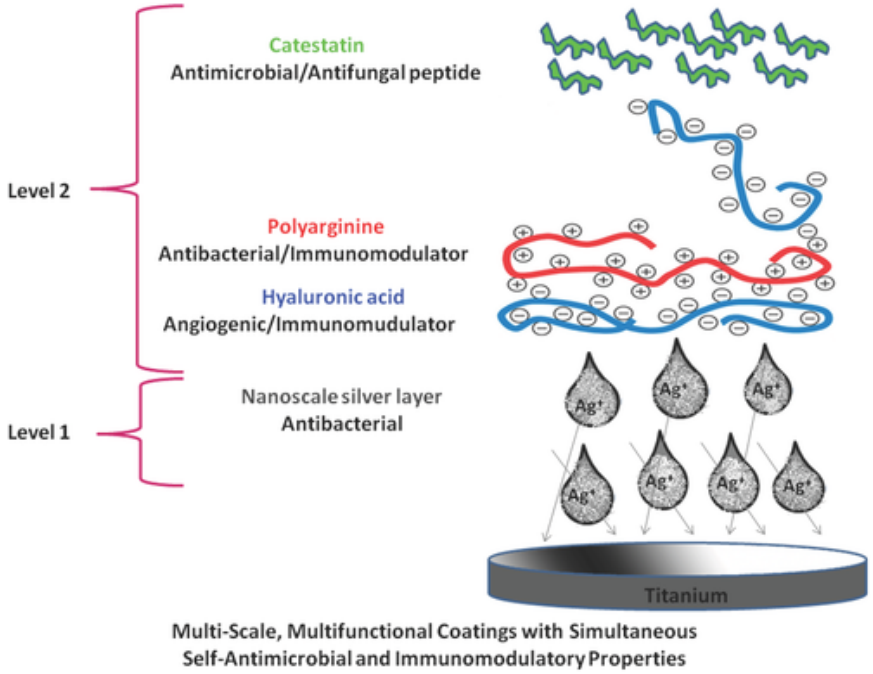

Figure 13: Example of polyelectrolyte multilayer (PEM); The multilayer film is based on polyarginine and hyaluronic acid [40].

However, because coatings have inherently limited reservoirs of antibacterial agents, their action is ultimately only temporary.

2.2.5.2 Contact-killing surfaces

Contact-killing coatings have been developed to circumvent the issue of reservoir exhaustion for the release-based coatings [41]. In this approach, antimicrobial compounds are covalently anchored to the material surface by flexible, hydrophobic polymeric chains [39]. Adhered bacteria are believed to be killed due to disruption of their cell membrane by the attached compounds, reaching across the microbial envelope thanks to the long tethering chains [40]. Because the main mechanisms of action are based on membrane interactions, such as physical lysing or charge disruption, the most effective compounds for contact-killing coatings have been either cationic compounds (QACs, chitosan, AMPs, etc.) or enzymes [43].

As an example, cationic surfaces with alkylated quaternary ammonium groups kill adhering bacteria upon contact membrane disruption and are considered increasingly promising as a non-antibiotic based way to eradicate bacteria adhering to surfaces [44].

The long-term efficacy of contact-killing surfaces is questioned because of a potential coverage of the surface by absorbed proteins from blood but also by the development of a layer of dead bacteria [38].

2.2.5.3 Non-adhesive surfaces

Contact-killing and non-adhesive surfaces are considered advantageous for long-term antimicrobial activity.

Anti-adhesion coatings seek to prevent the earliest step of biofilm formation using non-cytotoxic mechanisms. Surface immobilization of molecules that can resist protein adsorption, such as PEG and zwitterion, has demonstrated great anti-adhesion properties *in vitro*. Despite stability issues, they are generally regarded as the standard approach for anti-adhesion coatings [39].

However, the use of physical surface modifications (especially surface topography) as non-specific methods to modulate bacterial adhesion is most likely more complex than previously thought [45][46][47]. It has been demonstrated that surface topography plays a crucial role in the adhesion of bacteria. Indeed the adhesive behaviour of bacteria can be controlled by regulating the topography of a surface. A classification of biointerfaces into three categories has been elaborated to discuss the influence of the surface topography on bacteria adhesion. This classification is presented in Figure 14. Random surfaces, ordered surfaces and dynamic surfaces are illustrated. The classification is based on the size ratio between bacteria and topography i.e. it takes into account the patterns that are smaller than bacterial cells, patterns that are comparable to bacterial cells and patters that are larger than bacterial cells. The patterns can either be random or ordered.

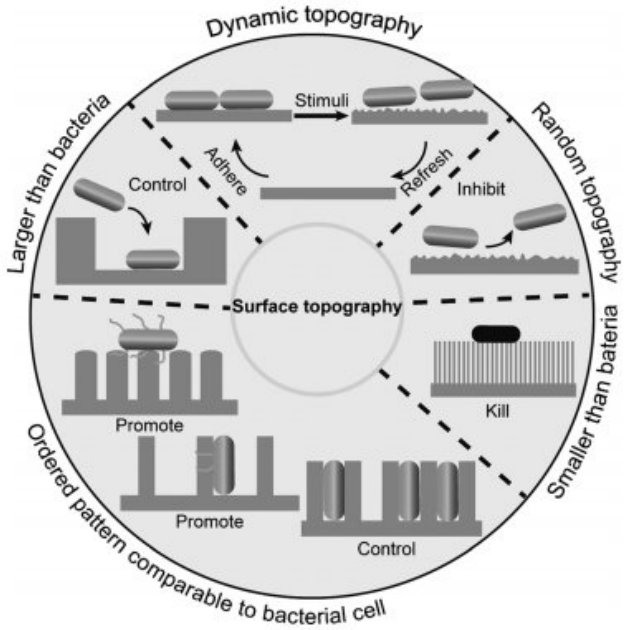

Figure 14: Classification of biointerfaces into three categories: random surfaces, ordered surfaces and dynamic surfaces [48].

Random surface topographies present a bacterial adhesion and colonization relatively unclear. In fact, the phenomenon of bacterial adhesion is ruled by the contact area between the bacteria

and the surface. Consequently, the variety of bacteria morphologies affects their adhesive behaviour on the surfaces. For example, spherical bacteria have a larger contact area on a rough surface than on a smooth. The opposite behaviour is observed with rod-shaped bacteria which adhere easily on smooth surfaces [48].

Moreover, the surface topography can be ordered to promote the control of bacterial adhesion repeating structural units. The subdivisions presented in Figure 14, allow to analyse the effect of bacteria microstructure, the interactions between bacteria and biointerfaces and the development of multicellular structures [48]. The topographic patterns smaller than bacteria cells have been developed taking inspiration from the nature as for example with the cicada wings or dragon wings [49]. Indeed, surfaces presenting nanopillars or nanowires possess bactericidal effect.

The bactericidal properties of surface topographies with smaller dimensions than bacterial cells are illustrated in the following figure, Figure 15.

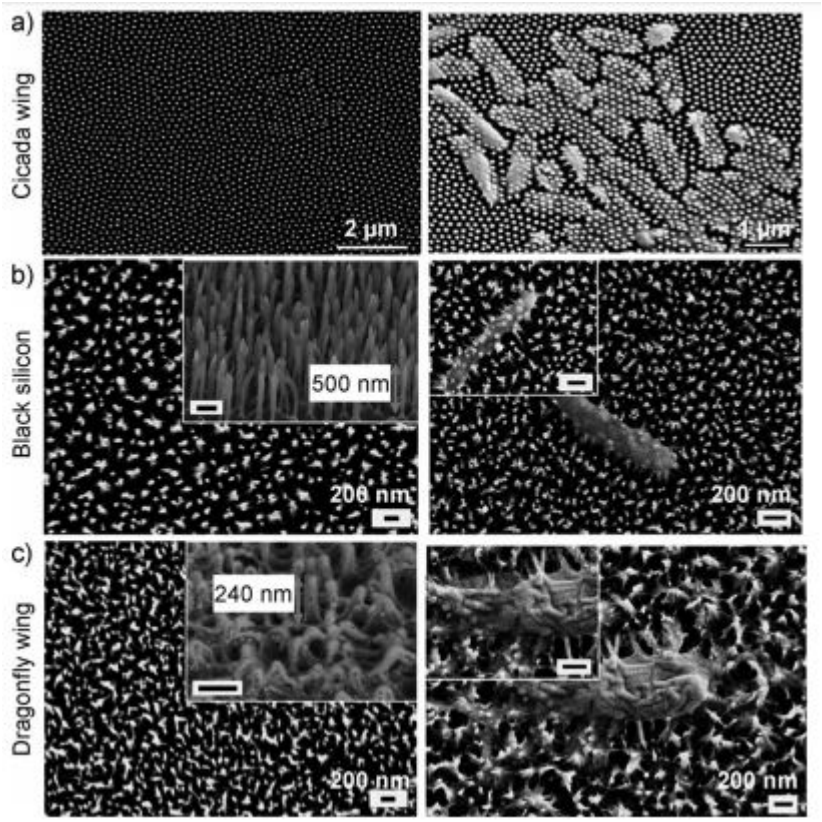

Figure 15: Bactericidal properties of surface topographies with smaller dimensions than bacterial cells. Surface topographies of cicada wings (a), black silicon (b) and dragonfly wings (c) are compared at different scales [48].

The elaboration of nanometer-scale periodic surfaces demonstrates that bacterial attachment and orientation can be modulated by nanoarrays. They can effectively inhibit biofilm formation.

In Figure 16, the adhesive behaviour of rod-shaped bacteria is analysed on surfaces whose topography have comparable dimensions to bacterial cells. In fact, the nanowire-arrays seem to perfectly control the orientation of the adhered bacteria. The bacteria are trapped in the arrays and it slows biofilm formation.However, with the aid of their flagella, some bacteria are able to overcome this kind of unfavourable surface topographies.

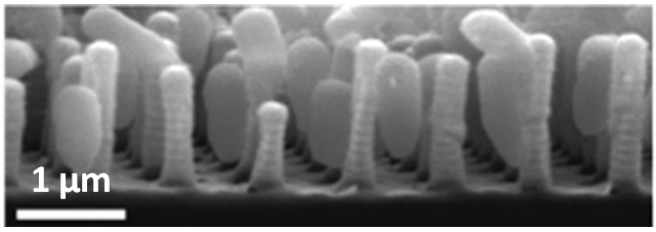

Figure 16: Bacteria orientation and adhesion controlled by surface topography comparable to bacterial size [50].

Finally, topographic patterns larger than bacterial cells allow to study multicellular structures. The topographies are generally governed by micrometer-sized patterns. The patterns are often pores or square-shaped. Bacteria adhesion is affected by the size of the patterns and the distance between the patterns. In Figure 17, three ranges of patterns are studied. The first range of pores analysed is inferior to 3,5 μm and it is observed a readily bacterial adhesion and biofilm formation. Besides, it is noticed that when the pores are larger within the range 5μm-11 μm, the bacterial activity could be effectively inhibited as the contact area is low. However, when the pores are larger than 11 μm, the bacteria are able to enter in the pores and proliferate without being disturbed [48].

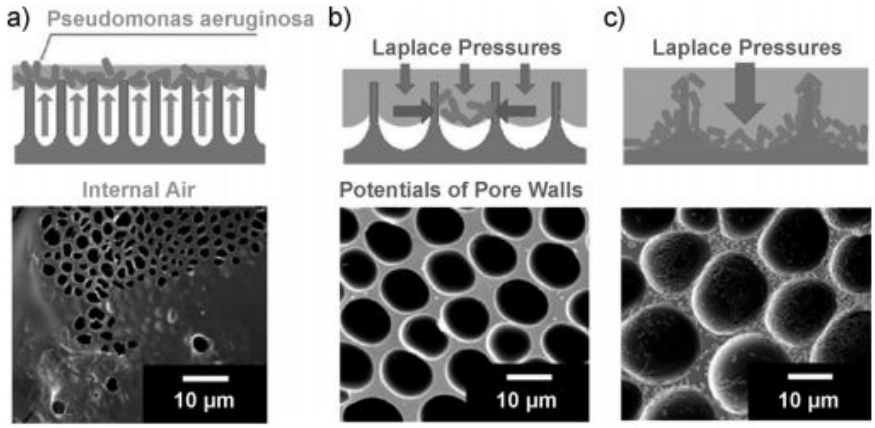

Figure 17: Influence of the patterns size on bacterial adhesion. Bacterial adhesion analysed on topographic patterns larger than bacterial cells at a range inferior to 3,5μm (a), at the range 5μm-11μ (b) and at a range superior to 11μm (c) [48].

The main issue of non-adhesive surfaces is that they are often also non-adhesive to tissue cells making them less suitable for biomaterial implants and devices requiring tissue integration as for bone regeneration [38].

3 Materials and methods

3.1 Calcium phosphates preparation

3.1.1 Preparation of alpha-tricalcium phosphate (α-TCP)

In order to elaborate the different biomaterials, the first step is to prepare the precursor phase: α-tricalcium phosphate compound α-$Ca_3(PO_4)_2$. To obtain this powder, calcium phosphate ($CaHPO_4$) and calcium carbonate ($CaCO_3$) in the form of solid powders are mixed in a 2:1 molar ratio of calcium phosphate compared to calcium carbonate. Consequently, 131,589 g of calcium phosphate (*Merck, ref: C7263, Lot MKBT9270V*) and 48,399 g of calcium carbonate (*Sigma Aldrich, ref: C4830, Lot SLBL4279V*) are put together. The mixing of these two powders is ensured by a vacuum power mixer (*WhipMix*) during 15 minutes. Nonetheless, in order to avoid an overheating of the mixer a break of one minute is done after 7 minutes.

When the powders are homogeneously mixed together, they are placed in a platinum crucible resistant to high temperature to perform the second step of the preparation, the sintering. The aim of the sintering is to transform the mixture of calcium phosphate and calcium carbonate into alpha-tricalcium phosphate (α-TCP), one of the high temperature forms of tricalcium phosphate.

The reaction is presented in the equation below:

$$CaCO_3 + 2CaHPO_4 \longrightarrow Ca_3(PO_4)_2 + CO_2 + H_2O$$

The thermal treatment is presented in Figure 18.

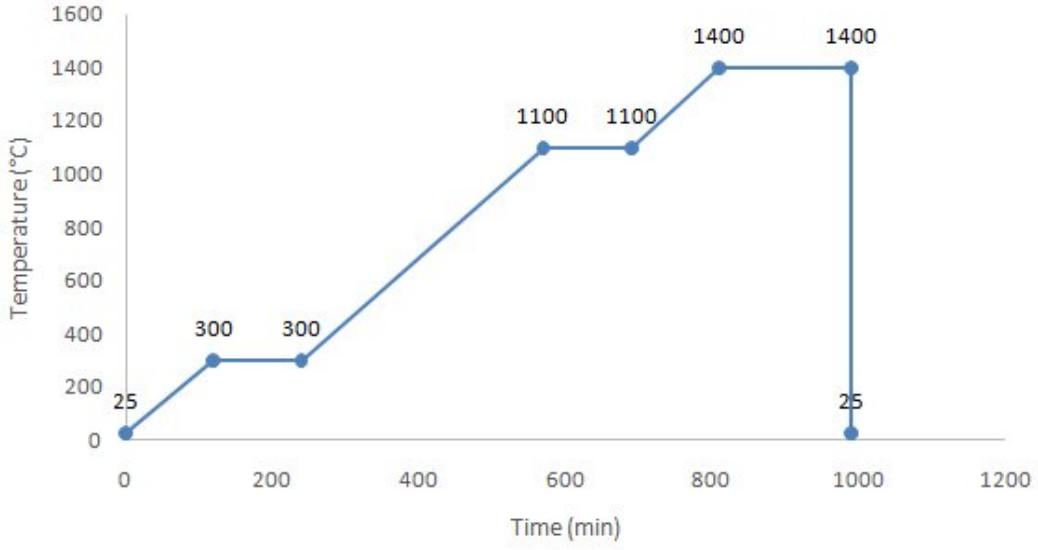

Figure 18: Thermal treatment for α-TCP.

High temperatures such as 1100°C and 1400°C have to be reached and applied for several hours to get α-TCP. Finally, a quenching needs to be done to stabilize the high temperature alpha-TCP phase. The quenching is executed taing out the crucible from the furnace (*Hobersal, CRN-58*) at 1400°C and breaking the compact powder into pieces to avoid transformation of phase to β-TCP. The whole thermal treatment lasts approximately 16 hours.

The next step is the milling of the α-TCP powder with a planetary mill *Fritsch*. Two sizes of particles are milled. The coarse powder with size of 5,8 μm and the fine powder with an average size of 2,4 μm. Therefore, the coarse powder is obtained using ten balls of a diameter of 30 mm. The milling is performed at 450 rpm during 15 min. Instead, the fine milling protocol requires more stages. The first stage is done using ten balls of a diameter of 30 mm at 450 rpm during one hour. The second stage is done milling with ten balls of a diameter of 30 mm but this time at 500 rpm and during 40 min. Finally, hundred of balls of a diameter of 10 mm are employed at 500 rpm during 60 min.

After the millings, a 2wt% of precipitated hydroxyapatite is added to the powders to accelerate the crystals' formation. In fact, the crystals of hydroxyapatite will play a part as nucleation sites and boost the crystallisation of the α-TCP.

3.1.2 Preparation of calcium deficient hydroxyapatite (CDHA)

The calcium deficient hydroxyapatite (CDHA) is obtained by hydrolysis of α-TCP according to the reaction:

$$3Ca_3(PO_4)_2 + H_2O \longrightarrow Ca_9(HPO_4)(PO_4)_5OH$$

Usually, α-TCP powder is mixed with water. However, the reaction is a reaction which lasts around ten days so it was decided to use an accelerant Na_2HPO_4 to reduce the reaction time to seven days. The accelerant is a solution of 2,5% in weight of Na_2HPO_4. After, the accelerant is mixed with the α-TCP powder at a liquid to powder ratio of 0,35 ml/g, the mixture is homogeneously mixed with a mortar and a pestle and transferred into teflon moulds of $\emptyset$ 6 mm by 2 mm height. Figure 19 illustrates this step.

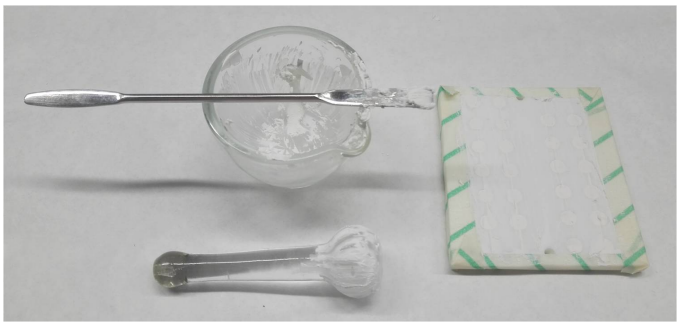

Figure 19: Equipment for the cementation reaction; Glass mortar and pestle, spatula and teflon mould (imprints of ∅ 6 mm).

Once the moulds are filled, they are allowed to set at relative humidity 100% at 37°C for several hours. After, they are disassembled and the CDHA discs are immersed in distilled water at 37°C for seven days. When the cement reaction is over, the discs are dried at 37°C. Figure 20 shows images of the set samples.

Figure 20: C-CDHA (left) and F-CDHA (right) discs

The CDHA compacted discs are fabricated by grinding and then compacting pre-set F-CDHA discs. The compacting is executed by a hydraulic press of the brand *Specac* presented in Figure 21.

Figure 21: Hydraulic press (*Specac*) employed for the powder compacting.

0,2 g of F-CDHA powder is placed in the press and compacted with a pressure of five tons during two minutes. Some compacted discs are presented in Figure 22.

Figure 22: Fc-CDHA discs

Finally, β-TCP discs are prepared by heat treatment of the C-CDHA discs at 1100°C for 15 hours. The thermal treatment is presented in Figure 23.

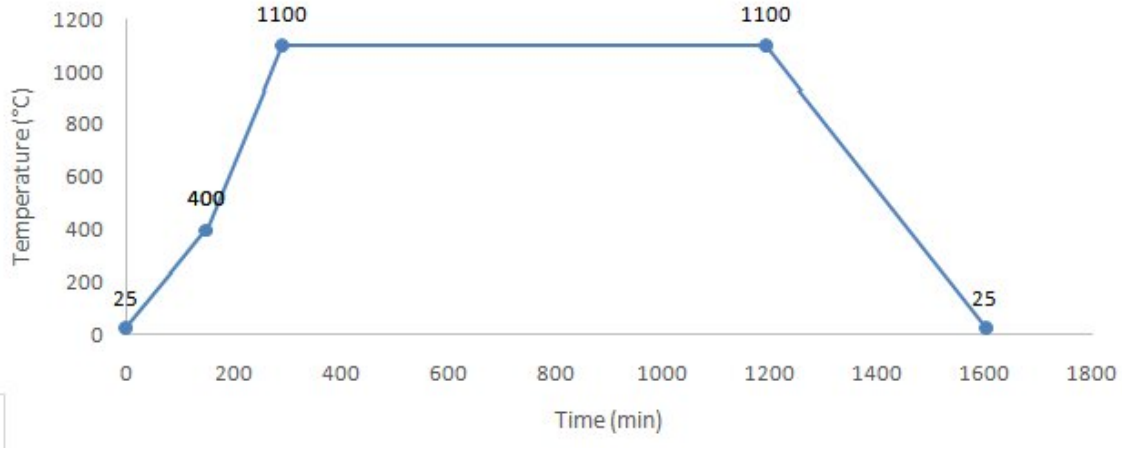

Figure 23: Thermal treatment for β-TCP.

The whole thermal treatment lasts approximately 30 hours and has a really slow cooling to be sure to only have the beta form.

Beta discs are shown in Figure 24.

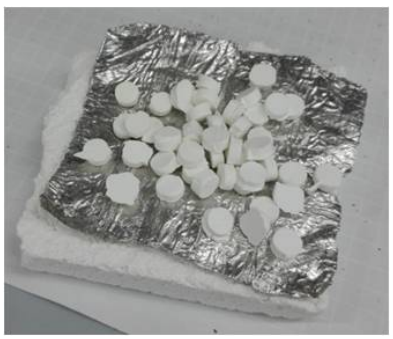

Figure 24: β-TCP discs

The sample codes are recalled below in Table 4.

Sample codes	Full name	Microstructure
C-CDHA	coarse calcium deficient hydroxyapatite	plate-like crystals
F-CDHA	fine calcium deficient hydroxyapatite	needle-like crystals
β-TCP	beta-tricalcium phoshate	polyhedral grains
Fc-CDHA	F-CDHA crushed and compacted	flat surface

Table 4: List of the different materials with associated codes and microstructure.

3.2 Physicochemical characterisation of CaPs

3.2.1 X-ray Diffraction (XRD)

3.2.1.1 Principle

X-ray diffraction is an analytical technique used for phase identification of a crystalline material. This technique is based on constructive interference of monochromatic X-rays and the crystalline sample. X-rays are generated by a cathode ray tube, filtered to produce a monochromatic radiation and directed toward the sample. The resulting interactions agree to the Bragg's law introduced below:

$$n\lambda = 2dsin\theta$$

The Bragg's law relates the wavelength of electromagnetic radiation λ to the diffraction angle θ and the lattice spacing d in a crystalline sample. The sample is scanned through a range of 2θ angles in order to determine all possible diffraction directions of the lattice.

3.2.1.2 Sample preparation

To analyse the crystalline phases of the different materials, a simple protocol is performed. The discs of C-CDHA, F-CDHA and β-TCP are grinded in an agate mortar to make them in the powder state. Then, the powders are respectively placed in an eppendorf. Figure 25 presents images of the preparation steps. The powders are then analysed in a diffractomer *D8 Bruker*.

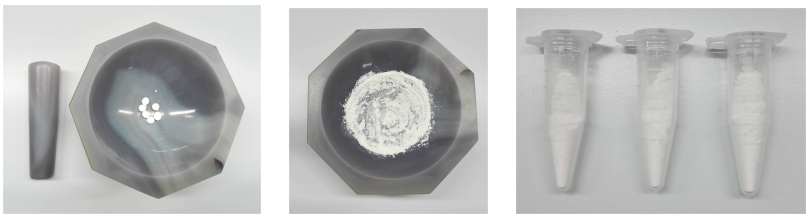

(a) Agate mortar and pestle with C-CDHA discs ready to be grinded.

(b) Agate mortar with C-CDHA powder.

(c) Eppendorf respectively filled with C-CDHA powder, F-CDHA powder and β-TCP powder.

Figure 25: Main preparation steps for DRX analysis.

3.2.2 Scanning electron microscopy (SEM)

3.2.2.1 Principle

Scanning electron microscopy is a technique capable of producing high resolution images of the surface of a sample using the principle of electron-matter interactions. The interactions are detected by a sensor that controls the brightness of a cathode oscilloscope whose scanning is synchronized with the one of the electron beam. As a result of these interactions, three types of particles will be analyzed: secondary electrons that are detached from the atoms of the material after collision with primary electrons, backscattered electrons and X-photons that come from the secondary electrons. Indeed, when an electron of the surface is detached (secondary electron), it is immediately replaced by another electron of the sample. This displacement of electrons is accompanied by an emission of a photon, an X photon. In the case of the project, the analysis by secondary electrons is elected due to the optimal resolution of the images.

3.2.2.2 Sample preparation

To analyse the surface of the raw biomaterials, scanning electron microscopy (SEM) tests are consequently executed by the machine *Phenom XL SEM*. The samples need to be prepared before the analyses. In fact, they are ceramics, so not electricity conductors what is necessary for SEM tests. To make the samples conductor, a carbon tape is firstly stuck on a metallic support called pin. The disc is then fixed on it as it is adhesive. To improve the conductibility, the top of the discs is linked to the tape thanks to a sliver solution (*Ted Pella, Lot 137876310*), as shown in Figure 26. Finally, the discs are covered by a carbon coating by the carbon coater *Emitech K950X*.

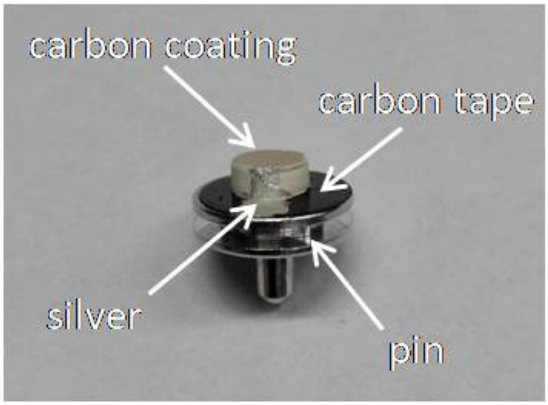

Figure 26: Non-conductor sample preparation for SEM analysis

For biological samples, i.e. the discs with adhered bacteria, a dehydration is previously required. The dehydration is a graded series of ethanol at 50%, 70%, 90%, 96% and absolute ethanol (*PanReac Applichem, Lot 0000936500*). Each solution is applied to the samples during 15 minutes. A graded series of ethanol avoids a too high osmotic pressure and to

damage the bacteria cytoplasmic membranes. Then, the samples are let at 37°C several hours to perfectly dry. Finally, they are sputtered with carbon coating to make them suitable for SEM visualization.

3.3 Bacterial assays

3.3.1 Bacterial essay preparation

The *Staphylococcus aureus* strains are kept in a petri dish at 8°C. The first step of the adhesion tests is to prepare a suspension of bacteria. A solution of nutrients is performed to fulfill all the needs of the bacteria. It has been demonstrated in different studies that *Staphylococcus aureus* develop well in a Brain Heart Infusion (BHI) environment. To prepare this solution, 9,25 g of BHI powder (*Scharlau, ref: 02-599-500, Lot 105117* are diluted in 250 mL of distilled water and sterilized in autoclave. One or two colonies of *Staphylococcus aureus* are taken off the petri dish and put in 10 mL of the BHI environment. This flask is then placed at 37°C in an incubator during a night to allow the bacteria to develop.

The bacteria concentration which will be in contact with the biomaterials is elected at 10^8 Colony Forming Units (CFU/mL). It is known that this concentration corresponds to an absorbance included in the interval [0,19;0,21]. To exactly know the concentration of the bacterial solution, measures of absorbance at 600 nm need to be done. Consequently, 2 mL of the solution of developed bacteria is diluted in 10 mL of BHI environment to reduce the high concentration of the proliferation solution. A series of absorbance tests is then executed to obtain an absorbance included in the interval [0,19;0,21]. The absorbance measures are taken with a *MicroSpek DSM Laxco* densitymeter.

Before being in contact with the bacterial solution, the samples are sterilized immersion in a 70% alcohol solution during several hours and then dried in an incubator. This step reduces the probability of bacterial contamination. Once sterilized, a disc of each type of materials (C-CDHA, F-CDHA, β-TCP and Fc-CDHA) is placed in a 24 well-plate and 700 μL of the 10^8 CFU bacteria solution is added. The well-plate is finally placed in an incubator at 37°C during the elected incubation times.

3.3.2 Evaluation of bacterial surface coverage by Live/Dead staining

3.3.2.1 Fluorescent confocal microscopy

3.3.2.1.1 Principle

Confocal fluorescence microscopy is a microscopic technique that provides three dimensional optical resolutions. This technique is very common in bacteria counting and used in many researches [50][51][52].

In a confocal fluorescence microscope, the sample is illuminated by a laser of appropriate wavelenght. The laser produces the excitation of fluorophores through absorption and makes fluorescence detectable. A bacterial viability kit (*LIVE/DEAD Bac Light Thermofischer*) based on the integrity of the bacteria membrane is used to distinguish the dead and live bacteria on the surface of the discs. The kit is composed of two fluorophores: a red fluorescent stain propidium iodide (PI) and a green fluorescent nucleic acid stain (*SYTO 9, ref: L7007, Lot 1417666*). In fact, bacteria with a compromised membrane, dead or dying, will be coloured in red, while bacteria with an intact membrane will be coloured in green.

3.3.2.1.2 Sample preparation

At the end of each incubation time, the discs are cleaned by a solution of Phosphate Buffered Saline (PBS) (*Gibco Life Technologies, ref: 18912014, Lot 1928131*) which is a water based salt solution whose ion concentration matches those of the human body. The objective of the cleaning is to remove the unattached bacteria from the surface of the discs. The cleaning consists in making flown 1mL of PBS on each disc and to repeat this step three times very gently. Then, in order to avoid both bacterial growing and detaching during the microscopic analysis, the bacteria are fixed on the samples with a solution of glutaraldehyde (*Sigma-Aldrich, Lot BCBJ6765V*), a crosslinker possessing amino groups also present in the protein membrane of the bacteria. The discs are submerged in a volume of 700 of glutaraldehyde at 2,5% in weight, during 30 minutes at 4°C. Finally, they are cleaned with PBS solution to remove the excess of glutaraldehyde. Furthermore, the surface with the adhered bacteria is put in contact with a drop of 20 of the fluorescent reagent during 3 minutes. The time reaction has to be carefully respected because of the strong effect of the fluorescent reagent which can also cause the coloration of the samples and as a consequence a strong backgroung during image acquisition. The fluorescent reagent is also removed in making flown 1mL of PBS on each disc and repeating this step three times very gently.

3.3.2.2 Image processing and software analysis

3.3.2.2.1 Principle

The pictures taken with the confocal laser scanning microscope (*CLSM, LSM 800; Zeiss* are interpreted by the software ImageJ. The ImageJ is a multi-format and open source image processing and analysis software. Moreover, it is written in Java and allows the creation of plugins and macros. The purpose to image processing is to qualify the number of adhered bacteria on the surface of the samples.

3.3.2.2.2 Image processing protocol

First and foremost, a preparation of the pictures has to be done. ImageJ works with three different channels: the red one corresponds to the dead bacteria, the green one to the live bacteria and the grey one to the material. The images respective to the three channels are opened by the following instructions: “image”, “colors” and “split channels”. They are after ordered as to the right channels by the instructions: “image”, “colors” and “merge channels” in order to create a composite material. The channels can be observed changing the position of the cursor *c*. The different stakes can be analysed changing the position of the cursor *z*. Some examples of the changes of the altitude *z* are presents in the following image. The different stacks are compacted in one plan by the instructions: “image”, “stacks”, “z project” and choosing “max intensity”. The colour and the contrast can be adjust thanks to the instructions: “image”, “colors”, “channel tools” and “image”, “adjust”, “color balance”.

A partially automatic macro, created to accelerate the process, is presented below in Figure 27. It requires the user intervention because some steps are proper to each image and therefore necessitate user reflection.

```
1  //Images preparation//
2  open();
3  run("Split Channels");
4  waitForUser("Asignar correctamente");
5  run("Merge Channels...");
6  run("Z Project...", "projection=[Max Intensity]");
7  run("Channels Tool...");
8  run("Color Balance...");
9  waitForUser("Ajustar los colores y pulsar OK");
10 run("RGB Color");
```

Figure 27: Partially automatic macro for the images preparation (ImageJ)

Once this step is performed, the count of the bacteria can be achieved. The binarization of the images, the pixels only have two values 0 or 255, is done thanks to the instructions: “image”, “adjust” and “thresholding”. After that, the pixels with the 255 value are black and the pixels with the 0 value are white. In order to get the count optimal, the binary image is improved such as with the separation of the bacteria thanks to the instruction: “process”. “binary”.

"watershed". The size of the bacteria can also be elected with the instruction: "analyse", "analyse particles".

A completely automatic macro was created to optimize the efficiency of the analyses and is presented on the following picture, in Figure 28.

```
//Bacteria counting//
macro "Macro para contar bacterias [s]" {
open();
run("16-bit");
setAutoThreshold("Default dark");
//run("Threshold...");
setOption("BlackBackground", false);
run("Convert to Mask");
run("Watershed");
run("Analyze Particles...", "  display clear summarize");
}
```

Figure 28: Automatic macro for bacteria counting (ImageJ)

3.3.3 Quantification of adhered bacteria

3.3.3.1 Optical density analysis

3.3.3.1.1 Principle

The bacterial growth is determined by optical density measurements. Unlike the area coverage technique, this strategy is faintly used in bacteria counting and innovative for the current period.

The equipment is an UV-visible spectrophotometer based on the absorption of an emitted light. The turbidity of the samples is measured at a single wavelength of 600 nm elected to be at the approximate size than the bacteria. Once emitted, the light interacts with the bacteria in solution which absorb a part of it. The rest of the signal is read by a detector and analysed.

3.3.3.1.2 Protocol

To evaluate either the bacteria are affected by the topography of the studied biomaterials during the adhesion tests, kinetic experiments are performed. The topography of the biomaterials has various effects on the membrane of the bacteria, for instance it could damage bacteria membrane. Knowing that at the beginning of the adhesion tests the initial concentration is equal to 10^8 Colony Forming Unit (CFU) for all samples, the strategy is to determine the final concentration of bacteria for each biomaterial at the end of the adhesion tests thanks to optical density measurements. The advantage on the adhesion and proliferation essays analysed by fluorescent confocal microscopy is that optical density measurements offer quantitative results. As an other approach, they can be compared to the previous qualitative results.

The bacteria detachment is realised thank to a vortexer *BR 2000 Bio rad*. Two times of vortex are elected to detach the bacteria from the biomaterials, 30 seconds and 120 seconds. Compacted discs cannot be studied due to their high fragility; they will not resist to the vortex and break.

In order to analyze all the factors that come into play in the adhesion and proliferation experiments, seven conditions, presented below, are put in place and analyzed by optical density measurements.

A) Samples with *Staphylococcus aureus* $\xrightarrow{vortex}$ Detached SA

Condition A allows the observation of the bacterial growth over time in contact with the detached crystals. The lag phase, the log phase, the stationary phase and the death phase will be determined.

B) Samples with BHI media (control 1) $\xrightarrow{vortex}$ Crystals suspension: crystal control

Condition B is a control to test the crystals effect. It verifies the potential effect of the crystals on the solution turbidity.

C) *Staphylococcus aureus* with condition B (control 2) $\xrightarrow{vortex}$ Crystals suspension: SA + crystal control

Condition C, which is the condition B with a known concentration of *Staphylococcus aureus*, enables the analysis of the crystals effect on the bacterial growth after applying vortex.

D) *Staphylococcus aureus* with B (control 3) $\rightarrow$ Crystals suspension: SA + crystal control ($\emptyset$ vortex)

Condition D, which is the condition B with a known concentration of *Staphylococcus aureus*, enables the analysis of the crystals effect on the bacterial growth without applying vortex.

E) *Staphylococcus aureus* with media (control 4) $\rightarrow$ *Staphylococcus aureus* suspension: SA

Condition E allows the observation of bacterial growth in their most favorable environment (without detached crystals) and without having been in contact with biomaterials. It represents common bacterial growth at 10^8 CFU.

F) BHI media (control 5)

Condition F is a control to detect bacterial contamination.

G) Calibration curve

Condition G allows the development of the calibration curve. To construct this curve, eight dilutions of bacterial suspension are carried out. The turbidity of the 10^1 CFU, 10^2 CFU, 10^3 CFU, 10^4 CFU, 10^5 CFU, 10^6 CFU, 10^7 CFU, 10^8 CFU concentrations is then measured in order to create the calibration curve. From this curve, it is then possible to determine the CFU concentrations of C-CDHA, F-CDHA and β-TCP measured in Condition A knowing their turbidity.

These conditions, once prepared in distinct and sterile eppendorfs, are then placed in a 96 well-plate to measure their turbidity over time by a microplate reader (*SynergyHTX*). Measures are taken each 15 minutes as measurement interval and the whole analysis lasts around 15 hours.

At the end of the measurements, the results can be plotted by a data analysis and graphic design spreadsheet representing the optical density as a function of time.

3.4 Statistical analysis

All statistical analyses are performed using SPSS software (IBM SPSS, Armonk, NewYork, USA). The data presented in graphs represent mean ± standard deviation (SD) (n=3). Normality is checked through the Shapiro–Wilk test. Statistical differences between groups for non-parametric data are analysed through Mann-Whitney U test. The level of significance for all tests is set at $p < 0.05$.

4 Results and discussion

4.1 Physicochemical characterisation of CaPs

4.1.1 X-ray Diffraction (XRD)

X-ray diffraction analysis allows phase identification of the different calcium phosphate substrates. Figure 29 shows that none of the materials is phase-pure as traces of unreacted α TCP are observed for the C-CDHA, the F-CDHA and the β-TCP.

Moreover, the β TCP diffractogram shows sharp diffraction peaks whereas broad peaks are observed for the C-CDHA and particularly for the F-CDHA. This i explained by the differences in the processing temperature of the materials. The high processing temperature of β-TCP at 100°C allows atom diffusion and facilitates crystal growth. As a result crystallinity increases and this is reflected in the sharpness of the peaks. Conversely, the lower the processing temperature is (37°C for C-CDHA), the least crystalline the materials becomes and broader XRD are obtained.

Besides, X-ray diffraction results notice that the sintered β-TCP is the most crystalline material compared to the calcium deficient hydroxyapatites as the peaks height is more significant. In other words, F-CDHA is less crystalline than the others.

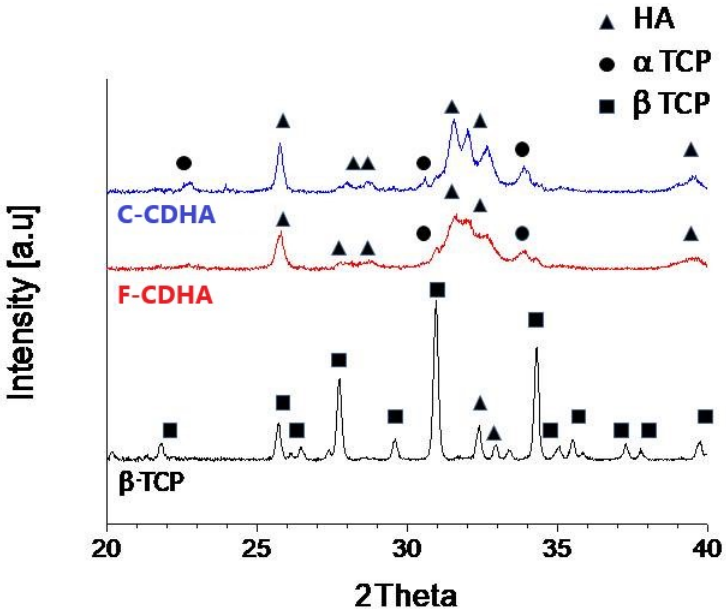

Figure 29: XRD patterns of the different calcium phosphates, from the top down: C-CDHA, F-CDHA and β TCP; The 2 θ measures have been taken between 20° and 40°. The geometrical forms correspond to the patterns of HA (01-086-1201, triangle), α TCP (01-070-0364, circle) and β TCP (01-070-2065, square).

4.1.2 Scanning electron microscopy (SEM)

The SEM micrographs of the calcium phosphates, presented in Figure 30, reveal major differences in terms of topography.

Despite C-CDHA and F-CDHA are two chemically identical compounds, their microstructure is completely different. C-CDHA is made of plate-like crystals whereas F-CDHA consists of needle-like crystals organized in agglomerates. The plate-like crystals are of the micrometric size whereas the needle-like crystals are nanometric. Besides, β-TCP, due the sintering process, presents a topography made of polyhedral grains of micrometric size. Finally, the Fc-CDHA substrate, prepared by hand milling of F-CDHA followed by compacting the crushed powder, has the smoothest surface without bumps among materials. A common feature in all materials (C-CDHA, F-CDHA and β-TCP) is the presence of pores which is inherent to the process: β-TCP is obtained by powder sintering while C-CDHA and F-CDHA are obtained by hydrolysis of α-TCP powders of different sizes.

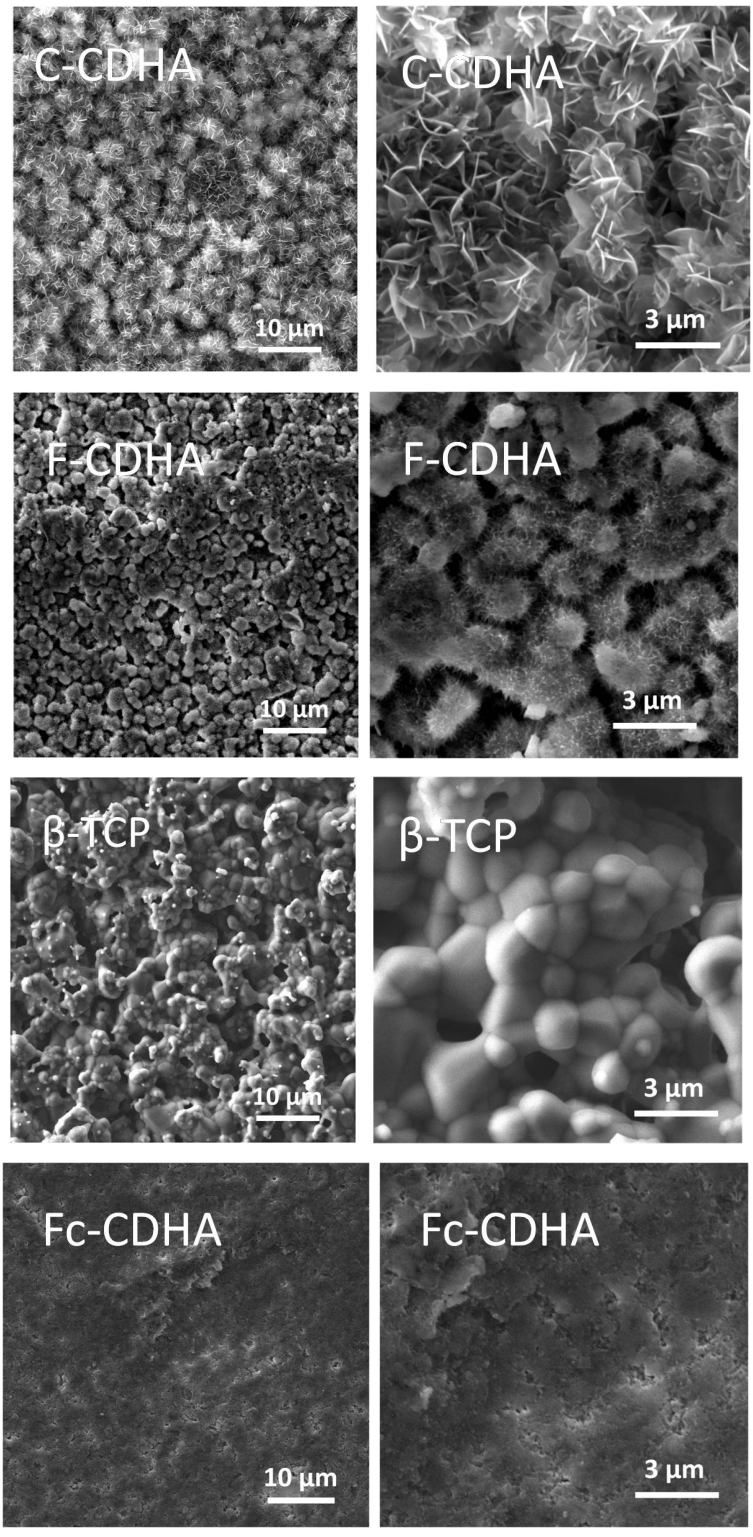

Figure 30: SEM micrographs of C-CDHA, F-CDHA, β-TCP and Fc-CDHA.

4.2 Bacteria assays

4.2.1 Evaluation of bacterial surface coverage by Live/Dead staining

4.2.1.1 Fluorescent confocal microscopy

In order to study bacterial adhesion on the surface of C-CDHA, F-CDHA, β-TCP and Fc-CDHA materials, representative images of each material have been taken by fluorescent confocal microscopy and are presented in Figure 31. The bacteria, stained in green by the dye, are clearly distinguishable from the material. However, if the interaction of the dye with the material was allowed for long time it would also color the material which complicates the analysis. Particular care was taken to this to not occur.

By visual analysis, it was observed that bacterial adhesion was rather homogeneous on the surface of the different materials.

However, it is clear that the proportion of adhered bacteria changes with the material being the most important for the β-TCP. Indeed, at 4 hours the number of bacteria is the highest among the materials at this point and increases significantly at 48 hours. On the contrary, the F-CDHA material has the smallest amount of bacteria adhered to its surface. A slight increase can be noted between 4 hours and 48 hours. As for the C-CDHA and Fc-CDHA, a rather similar amount of bacteria than for the F-CDHA covers their surface after 4 hours of incubation. However, after 48 hours, the number of bacteria has significantly increased. Nevertheless, the proportion of bacteria noticed on these two materials is lower than observed on the β-TCP material.

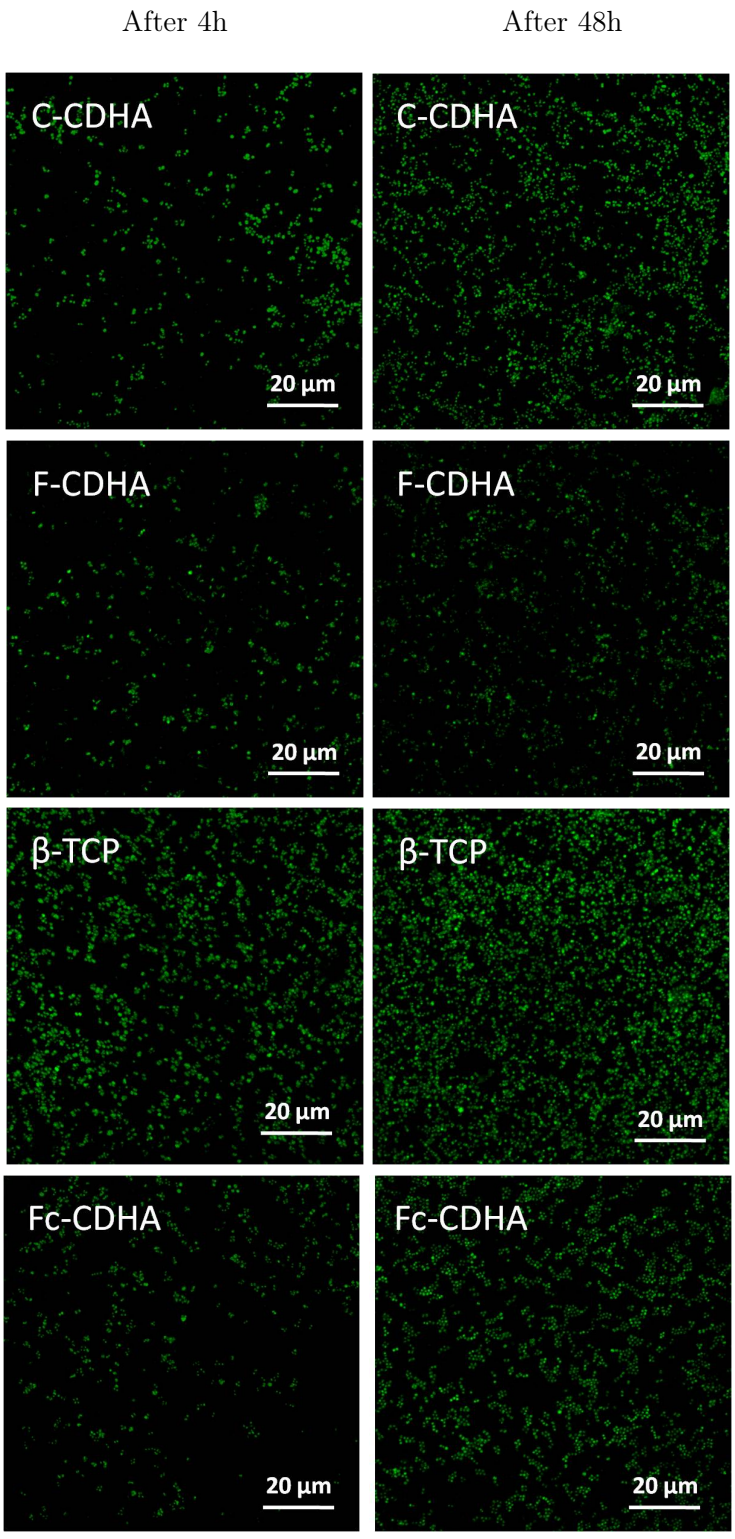

Figure 31: Images obtained by fluorescent confocal microscopy using Live/Dead staining. C-CDHA, F-CDHA, β-TCP and Fc-CDHA are presented after 4h (left) and 48h (right) of incubation with SA.

4.2.1.2 Image processing and software analysis

In order to semiquantitatively determine the percentage of adhered SA on the surface of the different samples, image analysis was performed. Prior to analysis, the bacteria were stained in green with Live/Dead staining. Subsequently, fluorescent images were taken and the percentage of green area was calculated. At least, three images were analysed per sample.

The results obtained are given in percentage of the surface coverage and collected in Figure 32. Graphs a) and b) correspond to two independent tests of *Staphylococcus aureus* adhesion and proliferation on C-CDHA, F-CDHA, β-TCP and Fc-CDHA materials assessed at 4 hours and 48 hours. On the other hand, graph c) corresponds to a test of *Staphyloccocus aureus* adhesion and proliferation on the same materials at 4 hours and 24 hours respectively.

The goal of performing three independent experiments was to asses the reproducibility of the assays. In general, the results showed similar trends between experiments.

As expected, the percentage of occupied area by the bacteria increases with time, consistent with the results from Figure 32. Moreover in general, bacteria adhesion and proliferation on the surface of F-CDHA material was the lowest compared to the rest of materials. On the contrary, for the β-TCP and the Fc-CDHA materials, the bacterial behavior did not seem to be affected by their surface topographies since the percentage of average occupied area was relatively important regardless the substrate and increased significantly over time. The percentage of SA surface coverage for the β-TCP and the Fc-CDHA markedly exceeded 10% after 48 hours of incubation. Nevertheless, for the C-CDHA material, bacteria proliferation at 48 hours of incubation was close to 10%. Concerning the F-CDHA, the percentage of surface coverage is near 5%. Thus the general trend observed in regard to SA surface coverage on the different materials was F-CDHA $<$ C-CDHA $\leq$ Fc-CDHA $=$ β-TCP.

One aspect to note was the large standard deviations in the same conditions which can be explained by the porous nature of the samples. Porosity can indeed act entrapping bacteria masking the results as bacteria hidden in the pores would not be measured.

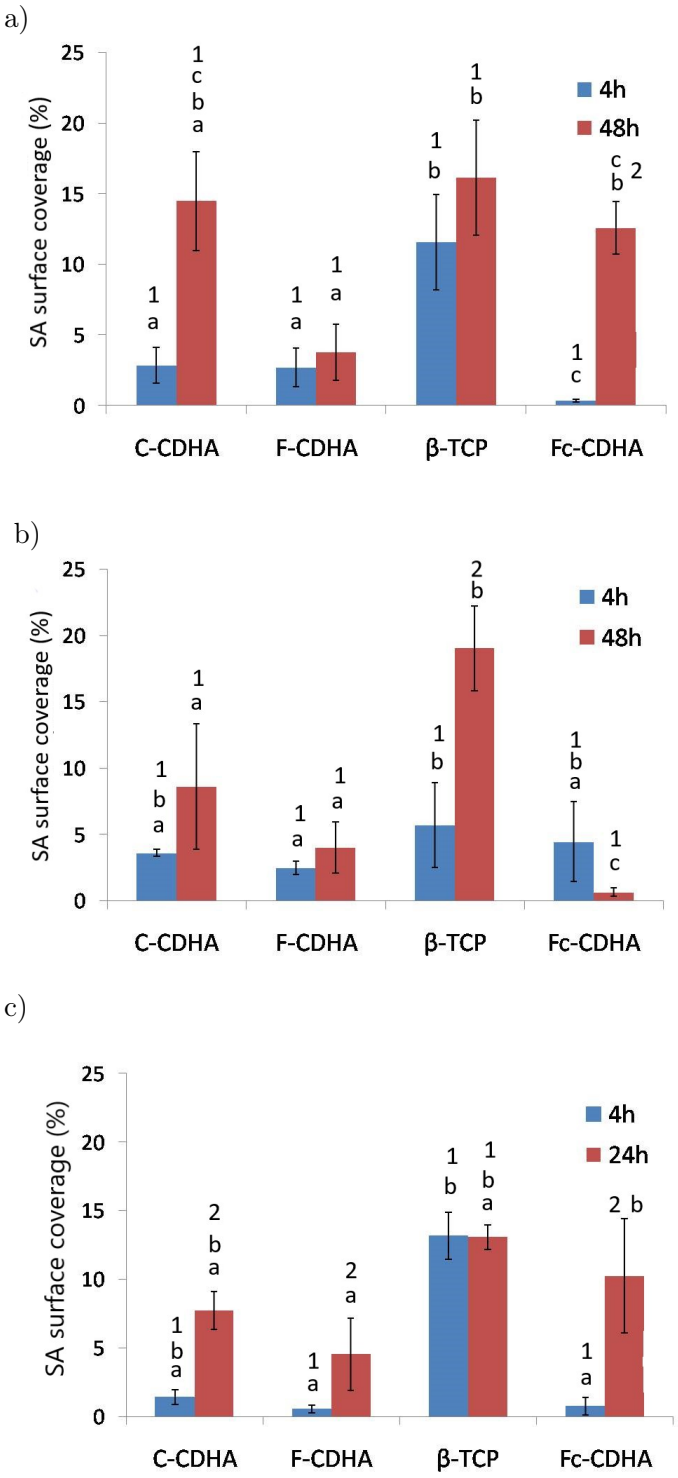

Figure 32: SA surface coverage (%) on C-CDHA, F-CDHA, β-TCP and Fc-CDHA at different time points. Graphs a, b and c correspond to three independent experiments. Error bar is the standard deviation of on average of 3 images. The same letter (a, b or c) indicates no statistically significant differences ($p > 0.05$) between substrates for each time point (either 4 hours or 48 hours (graphs a) and b)) or 24h (graph c)). The same number (1 or 2) indicates no statistically significant differences ($p > 0.05$) between time points for each substrate (C-CDHA, F-CDHA, β-TCP, Fc-CDHA).

Besides analyzing the bacterial behavior at 4 hours and 48 hours, longer term studies were also performed. Several adhesion and proliferation experiments were performed up to 7-day incubation periods. Figure 33 shows the results obtained for one of these experiments.

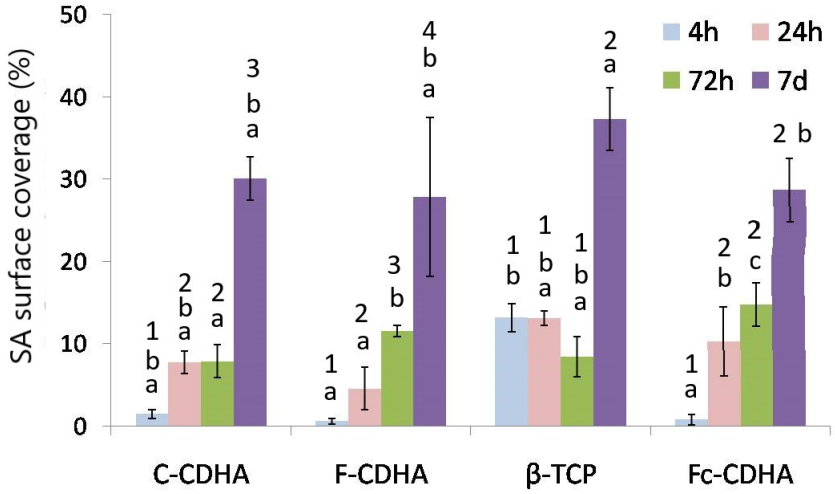

Figure 33: SA surface coverage (%) on C-CDHA, F-CDHA, β-TCP and Fc-CDHA after 4h (blue), 24h (red), 72h (green) and 7d (purple) of incubation. The same letter (a, b or c) indicates no statistically significant differences ($p > 0.05$) between substrates for each time point (either 4 hours, 24 hours, 72 hours or 7 days). The same number (1, 2, 3 or 4) indicates no statistically significant differences ($p > 0.05$) between time points for each substrate (C-CDHA, F-CDHA, β-TCP, Fc-CDHA).

It was striking to see that SA could not grow continuously. In part, in some samples between 24 hours and 72 hours, SA seemed not to grow. This was explained by the growth of SA forming multilayers on the surface of the materials. Each bacterium forms its colony and grows very rapidly in all directions (x,y,z) (Figure 35. However, the calculations of the percentage of surface coverage by computer analysis only allows an analysis in the plane xy. All the SA growing in the z direction can not be measured. Thus the results presented in Figure 33 are not truly representative, when this occurs it is meaningless to perform bacterial quantification analysis. Studies should be made before this occurs (i.e. within 4 hours and 48 hours).

Furthermore, in the long-term analysis it was detected bacteria detachment from all materials as assessed by the cloudiness of the cell culture medio in contact with the samples in Figure 34. Bacterial detachment is a natural phase in the bacteria growth. Unfortunately, assessment of SA proliferation in long-term assays are not meaningful.

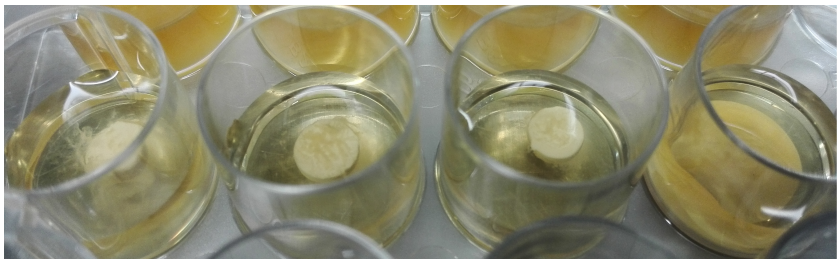

Figure 34: The detachment of the extracellular matrix on C-CDHA, F-CDHA, β-TCP and Fc-CDHA (from right to letf) after 72h of incubation with SA is observed by the clouding of the solution.

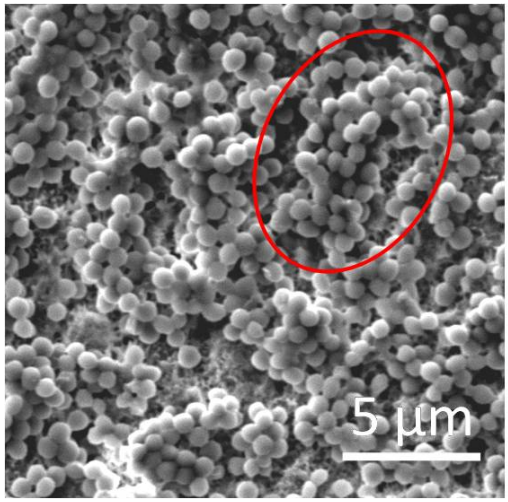

Figure 35: SA growth on F-CDHA after 6 days demonstrating the ability of SA to grow on the (x, y, z) directions.

4.2.1.3 Scanning electron microscopy (SEM)

SEM micrographs of the calcium phosphates after bacterial adhesion and proliferation tests allowed the observation of the adhered SA and the materials. The preferred location of SA on the different topographies can be observed. The SEM micrographs presented in Figure 36 compare the bacterial adhesion and proliferation between two times, 4 hours and 24 hours of incubation.

The SEM results agreed well with the results obtained by L/D staining. In addition, it was possible to observe that after 4 hours, the bacterial adhesion on the β-TCP was preferentially located in the pores whereas it was completely widespread on the surface after 24 hours. For the C-CDHA samples, the bacteria were either entrapped between the crystals aggregates but they were also found to adhere on the surface of the plate-like crystals (this was more evident after 24 hours of incubation). On the F-CDHA samples bacteria were mostly entrapped within the large pores. They could not penetrate the network of needle-like crystals due to the large size of bacteria compared to the crystals. Finally, the bacterial adhesion on the Fc-CDHA was particularly difficult after 4 hours as the surface was too flat which made adhesion hard. However after 24 hours, the adhered SA had grown rapidly on the surface. Thus, the limitations of all the materials in terms of antimicrobial properties come from the pores between the particle aggregates. The pores trap the bacteria and promote their adhesion and thereafter their proliferation.

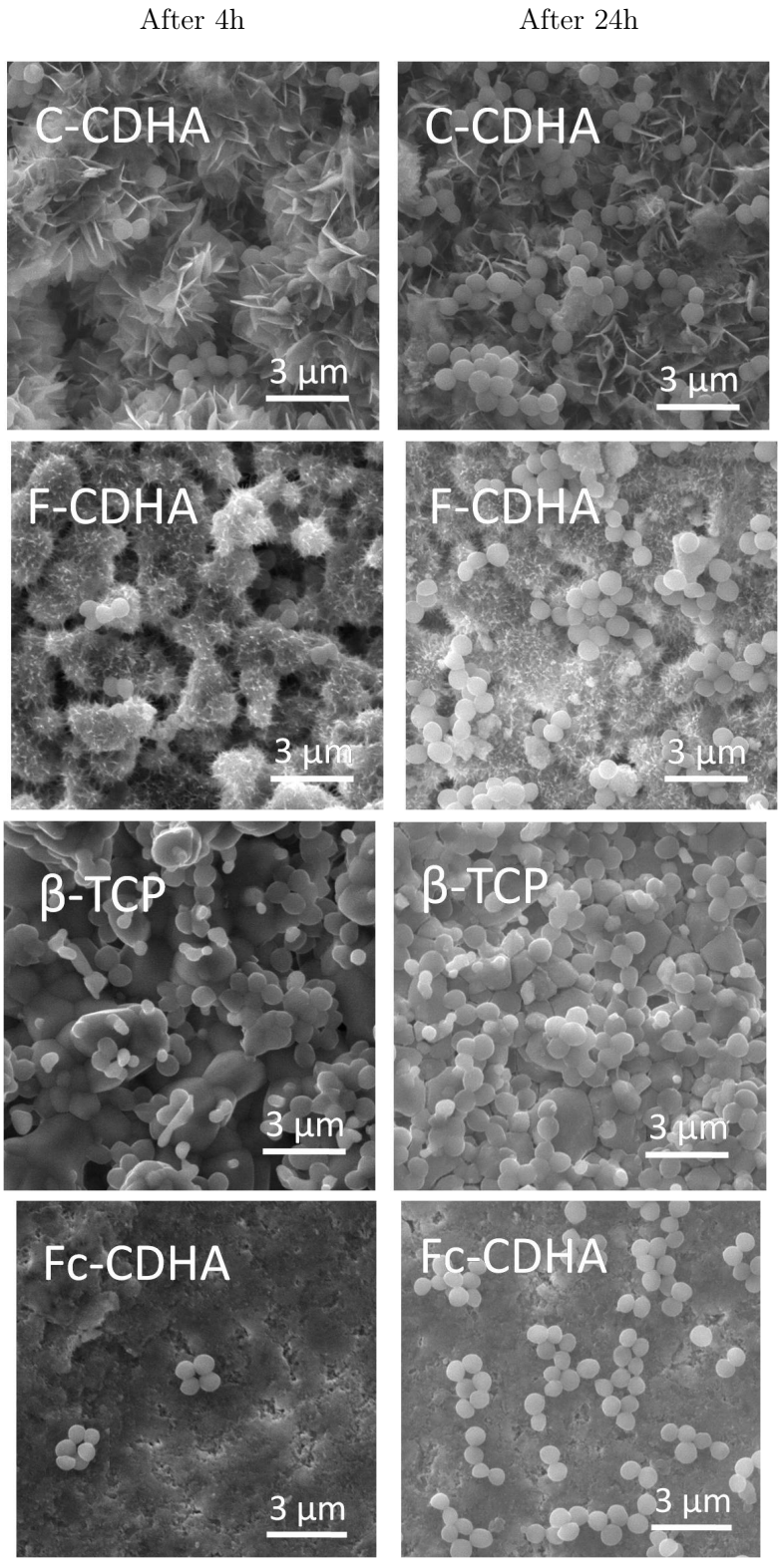

Figure 36: SEM micrographs of C-CDHA, F-CDHA, β-TCP and Fc-CDHA after 4h (left) and 24h (right) of incubation. Scale bar of 3 μm.

4.2.2 Quantification of adhered bacteria

To overcome the limitations of the semiquantitative studies obtained by image analysis (i.e., the difficulty in analysing bacteria located within pores and the fact that SA pile up in the z direction is not taken into account) and to validate the short-term results, quantification of SA on the samples was attempted by detaching the bacteria and following their growth curve in a spectrophotometer. This strategy is based on the measurement of the turbidity or the optical density of a suspension of cell mass or cell number.

Figure 37 gathers the different optical density measurements after a *Staphylococcus aureus* adhesion test at 4 hours on C-CDHA, F-CDHA and β-TCP. The bacteria are detached by a 30 seconds or 120 seconds vortex. Compacted samples could not be studied due to their high fragility; They could not resist the vortices.

For this experiment, three conditions (A, B and C) were analysed for the two vortex times.

These conditions are recalled below:

A) Samples with *Staphylococcus aureus* $\xrightarrow{vortex}$ Detached SA: SA + crystals

Condition A allows the observation of the bacterial growth over time in contact also with the detached crystals. This is due to the fact that vortex besides detaching SA also breaks down crystal agglomerates. The lag phase, the log phase, the stationary phase and the death phase will be determined.

B) Samples with BHI media (control 1) $\xrightarrow{vortex}$ Crystals suspension: crystals control

Condition B is a control to test interference of the crystals during measurement. It verifies the potential effect of the crystals on the solution turbidity.

C) *Staphylococcus aureus* with condition B (control 2) $\xrightarrow{vortex}$ SA with crystals suspension: SA + crystals control

Condition C, which is the condition B with a known concentration of *Staphylococcus aureus*, it enables the analysis of the crystals effect on the bacterial growth after applying vortex.

Graphs a), b) and c) in Figure 37 are related to a vortex time of 30 seconds whereas graphs d), e) and f) to a vortex time of 120 seconds.

The bacterial growth (condition A) for the three samples C-CDHA, F-CDHA and β-TCP is presented in graphs a) after 30 seconds of vortex and d) after 120 seconds of vortex. The exponential growth curve observed accounted by the growth of SA detached from the samples and was naturally expected. Nonetheless, during the lag phase i.e., between 0 minutes and 200 minutes, unusual peaks were observed. These peaks were accounted for the interference

of the crystals detached during vortex. They affect the turbidity of the solution during approximately 200 minutes, a time which can be associated to their sedimentation. After this time, they lie on the bottom of the well plate and do not interfere anymore in the optical density measurements.

Graphs b) and e) in Figure 37 correspond respectively to the analysis of the crystals in the media, without *Staphylococcus aureus*, after 30 seconds and 120 seconds of vortex (condition B). These graphs allow to isolate the crystals effect from that of bacterial growth. It is noticed that the peaks associated to the interference of the detached crystals are even higher as the applied vortex time rises. For example, the turbidity of the detached crystals from the C-CDHA is around 0,4 after 30 seconds of vortex and increases to 1 after 120 seconds. The turbidity increase for the other materials was not as significant as with the C-CDHA crystals.

Graphs c) ad f) in Figure 37 correspond to the condition C. They represent the growth of known concentration of *Staphylococcus aureus* in contact with detached crystals from condition B and after applying 30 seconds of vortex (c)) and 120 seconds of vortex (f)). The presence of the crystals effect consequently modifies the positions of the curves presented on these graphs. Curves c) and f) should be perfectly identical, nevertheless a substantial displacement of the curve related to the CCDHA crystals effect is observed. This displacement distorts the results and could consequently lead to a false interpretation.

30 SEC VORTEX

a) Detached SA from samples

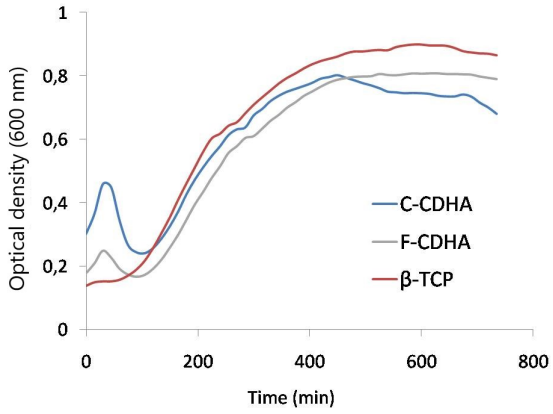

b) Control of crystal

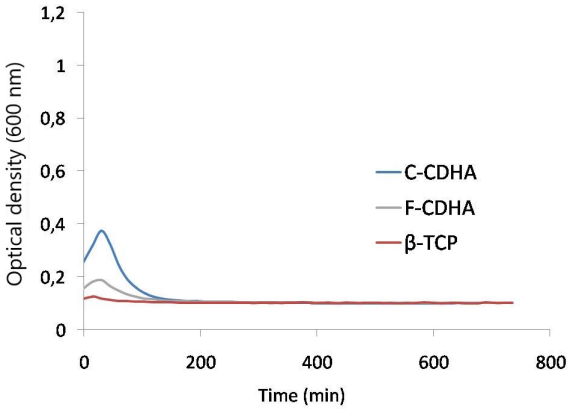

c) Control of crystal and SA

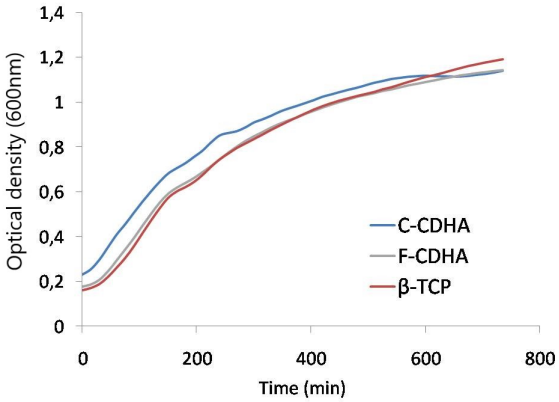

120 SEC VORTEX

d) Detached SA from samples

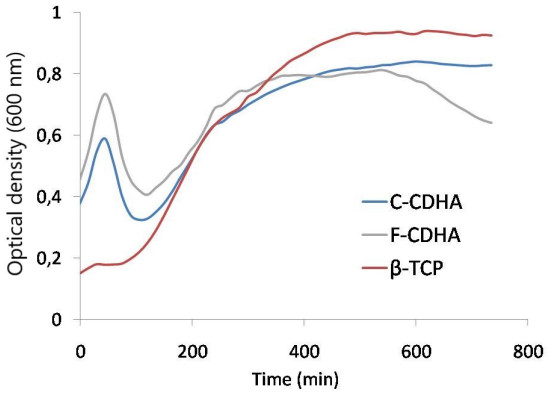

e) Control of crystal

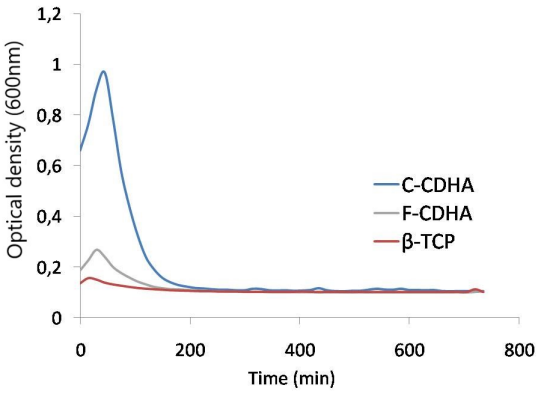

f) Control of crystal and SA

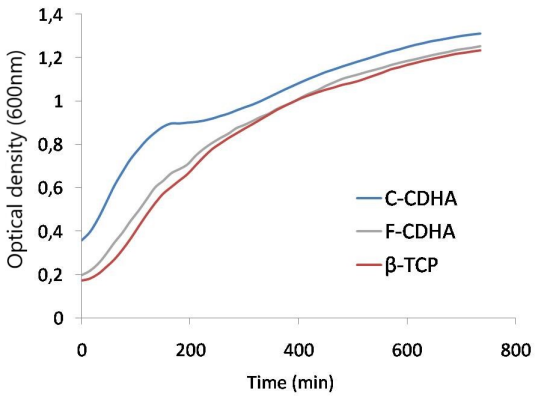

Figure 37: Optical density measurements after a *Staphylococcus aureus* adhesion and proliferation test of 4 hours on C-CDHA (blue), F-CDHA (grey) and β-TCP (red). a) Detached SA, 30 seconds vortex; b) Crystal control, 30 seconds vortex; c) SA + crystal control, 30 seconds vortex; d) Detached SA, 120 seconds vortex; e) Crystal control, 120 seconds vortex; f) SA + crystal control, 120 seconds vortex.

In order to confirm the detaching efficiency of SA by the action of the vortex, the samples underwent vortex at 30 seconds and 120 seconds were analysed by Live/Dead staining and the values of surface coverage were compared with the values obtained without vortex application. This was done for all materials except F-CDHA due to its fragility. SA incubation time was allowed for 4 hours. The results are presented in Figure 38 clearly prove a high detaching efficiency of SA already after 30 seconds vortex compared to the non-vortexed materials. In fact, after 30 seconds of vortex, less than a 0,5% of surface is covered by bacteria. These observations are confirmed with the low standard deviations. In fact, after short incubation times, the bacteria are mostly on the surface of the materials. SEM analysis of the samples confirmed that only a few SA remained hidden in the pores of the samples.

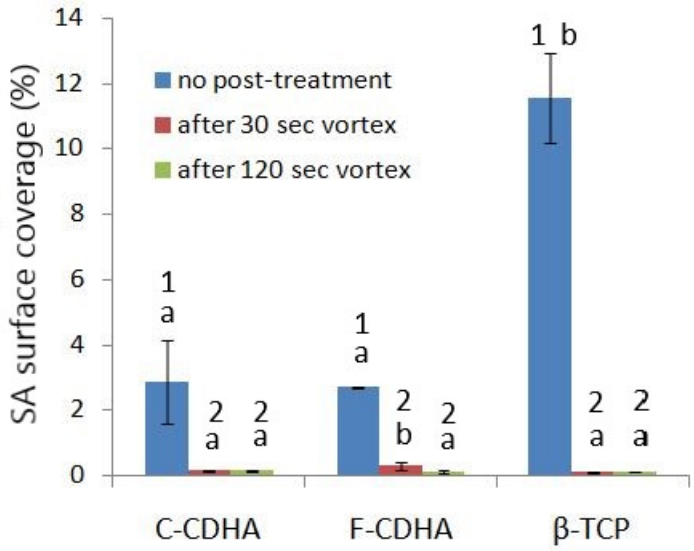

Figure 38: SA surface coverage (%) on C-CDHA, F-CDHA and β-TCP after a 4h adhesion test. Without post-treatment (blue, control sample), after 30 seconds vortex (red) and after 120 seconds vortex (green). The same letter (a or b) indicates no statistically significant differences ($p > 0.05$) between substrates for each post-treatment (either without, 30 seconds vortex or 120 seconds vortex). The same number (1 or 2) indicates no statistically significant differences ($p > 0.05$) between the post-treatments for each substrate (C-CDHA, F-CDHA, β-TCP).

Despite the success in the detaching efficiency, the results of SA growth curves in Figure 37 were distorted by the interference of crystals during the measurement. To prevent crystal contribution in the studies the following strategy was performed. It consisted in allowing the crystals to sediment before reading SA growth in the spectrophotometer. Since the contribution of crystals disappears after sedimentation ($\sim$ 200 minutes as observed in Figure 37), the samples were placed in the fridge for 700 minutes to allow crystal sedimentation while preventing SA growth. Afterwards, the samples were read in the spectrophotometer as usual. Figure 39 gathers the different optical density measurements of this experiment for the following conditions:

A) Samples with *Staphylococcus aureus* $\xrightarrow{vortex}$ Detached SA + crystals

Condition A) allows the observation of the bacterial growth over time in contact with the detached crystals. The lag phase, the log phase, the stationary phase and the death phase will be determined.

B) *Staphylococcus aureus* added to a suspension of crystals (control 2) $\xrightarrow{vortex}$ Crystals suspension: SA + crystals control

In condition B a known concentration of *Staphylococcus aureus* is added to the crystal suspension to assess the crystals effect on the bacterial growth.

C) *Staphylococcus aureus* with media (control 4) $\rightarrow$ *Staphylococcus aureus* suspension: SA

Condition C allows the obturbidityservation of bacterial growth in their most favorable environment (without detached crystals) and without having been in contact with biomaterials. It represents common bacterial growth at 10^8 CFU.

D) Bacterial growth curves

Condition D allows the development of the calibration curve. To construct this curve, eight dilutions of bacterial suspension are carried out. The turbidity of the 10^1 CFU, 10^2 CFU, 10^3 CFU, 10^4 CFU, 10^5 CFU, 10^6 CFU, 10^7 CFU, 10^8 CFU concentrations is then measured in order to create the calibration curve (Condition E). From this line, it is then possible to determine the CFU concentrations of C-CDHA, F-CDHA and β-TCP measured in condition A knowing their turbidity.

As desired, the crystals contribution on the SA growth was no longer observed thanks to the sedimentation step. The bacterial growth in the different conditions can now be observed without crystals interference. On graph a), the curves of C-CDHA, F-CDHA and β-TCP are identical. This indicates that a similar amount of SA was present in all materials. Comparing graph b) with graph c), no difference was found which indicates that the vortex of SA in he presence of crystals does not damage the bacteria.

Thanks to the representation of the dilution turbidity curves shown in graph d), it was possible to plot the calibration curve corresponding to an absorbance of 0.5, graph e). By selecting the time value corresponding to the absorbance of 0.5 on graph a) for the C-CDHA, F-CDHA and β-TCP curves and by putting this value on the calibration curve (Figure 39 e)), it was possible to determine the bacterial concentrations (CFU) specific to each material. The results of graph a) confirmed bacterial concentrations (CFU) of each material are very close around 3.10^6 CFU.

a) Detached SA from the samples

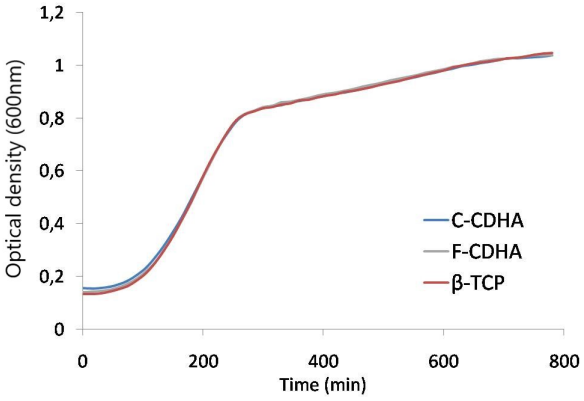

d) Bacterial growth curves

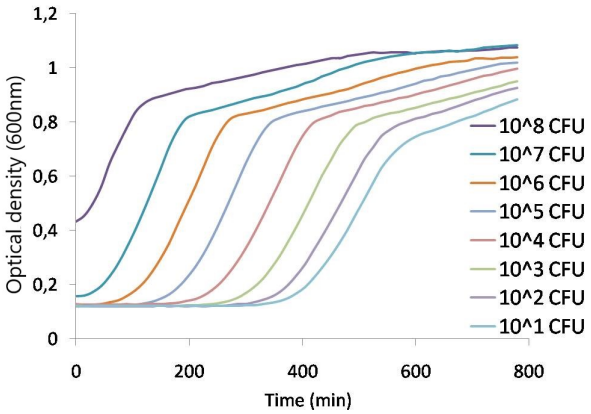

b) Control of crystal + SA

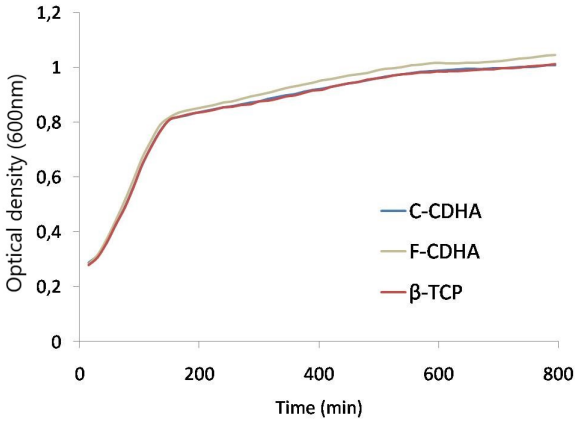

e) Calibration curve

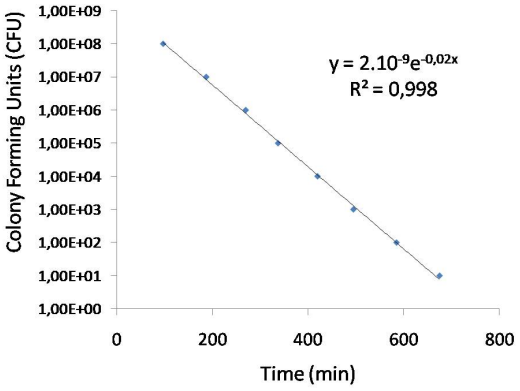

c) SA

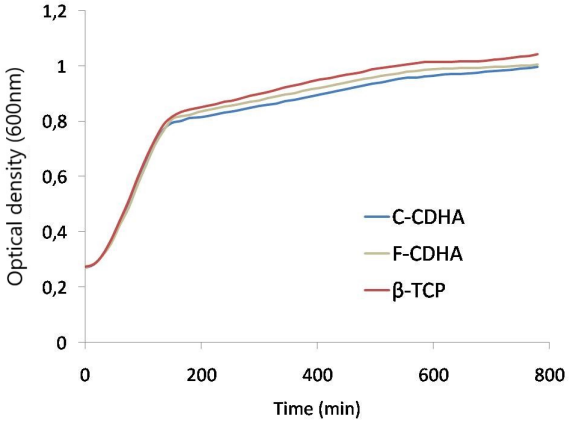

f) Number of SA detached from the samples

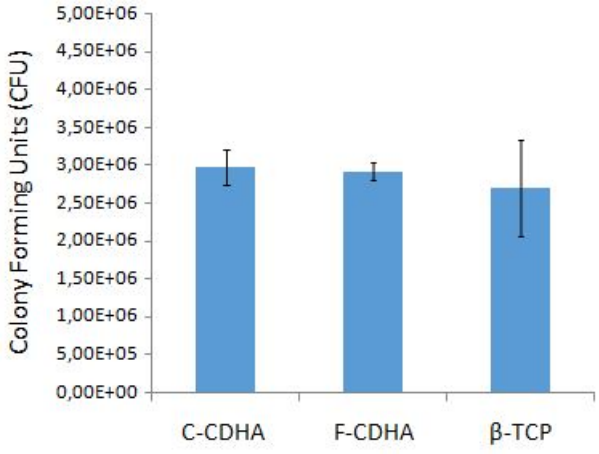

Figure 39: Optical density measurements after a *Staphylococcus aureus* adhesion and proliferation test of 4 hours on C-CDHA (blue), F-CDHA (grey) and β-TCP (red). Bacteria detachment: 30 seconds; a) Detached SA + crystals; b) Control of crystal + SA; c) SA d) Bacterial growth curves; e) Calibration curve; f) Number of cell detached from the samples.

It is interesting to compare the results obtained by the two methods used to measure adhered bacteria: Live/Dead staining versus optical density measurements. Optical density analysis is relatively innovative as few studies are present in literature that compare the results. That's why a comparison of the percentages of SA surface coverage by confocal microscopy and optical density was done. The comparison is elaborated after 4 hours adhesion.
The numerical data of the detached SA by a 30 second vortex are presented in Table 5 and they correspond to the results of the experiment in Figure 39.

Samples	Number of adhered bacteria (CFU)	Standard deviations (CFU)
C-CDHA	2 977 489	233 436
F-CDHA	2 915 614	119 672
β-TCP	2 704 942	636 355

Table 5: Number of adhered SA (CFU) on the samples C-CDHA, F-CDHA and β-TCP which were detached by a 30 second vortex after a 4 hour adhesion test.

Considering that the *Staphyloccocus aureus* are perfectly round, their diameter is considered of 1 μm. Thus a bacterium occupies an area of 0,7854 μm^2.
Moreover the samples C-CDHA, F-CDHA and β-TCP have a diameter of 6 mm. The total area is consequently 28,27.10^6 μm^2.
The data in Table 6 summarizes the total area occupied by the bacteria on the materials C-CDHA, F-CDHA and β-TCP along with the standard deviations.

Samples	Surface coverage (mm^2)	Standard deviations (mm^2)	Surface coverage (%)	Standard deviations (%)
C-CDHA	2,34	0,18	8,28	0,64
F-CDHA	2,30	0,09	8,14	0,32
β-TCP	2,12	0,5	7,50	1,77

Table 6: Quantification of SA surface coverage in mm^2 and % before SA detachment after a 4 hour adhesion test.

Thus, a comparison of the results of the two approaches, qualitative (Figure 32 graph b) and quantitative (Figure 39, graph f), for a 4 hour adhesion and proliferation test can be made. The respective results are presented in Table 7. First of all, Table 7 shows similar orders of magnitude for the results of the two approaches which confirms a coherence in the results. Nonetheless, the quantitative method shows higher percentages of surface coverage than for the fluorescence analysis. This can be explained by the limitations of the L/D staining which only takes into account the amount of SA projected in the 2D image. Instead, optical density measurements are considered to provide a more realistic amount of SA provided they are detached.

Moreover, unlike for the C-CDHA and F-CDHA, the percentages of surface coverage obtained for the β-TCP are very close for both quantification strategies. Indeed, the smooth topography of the β-TCP allows a better quantification of the adhered bacteria. Unfortunately, on the C-CDHA and the F-CDHA the presence of large pores might hide bacteria which can not be properly quantified by fluorescence imaging.

Samples	Surface coverage by confocal microscopy (%)	Surface coverage by optical density (%)
C-CDHA	3,61 $\pm 0,26$	8,28 $\pm 0,64$
F-CDHA	2,49 $\pm 0,51$	8,14 $\pm 0,32$
β-TCP	5,70 $\pm 3,19$	7,50 $\pm 1,77$

Table 7: Comparison of the SA surface coverage on the materials C-CDHA, F-CDHA and β-TCP after a 4 hour adhesion test determined by confocal microscopy (qualitative approach) and optical density (quantitative approach).

Thinking that a 4-hour experiment might not be long enough to allow the materials to act on the adhered bacteria, a longer kinetic experiment was this time performed. The adhesion and proliferation of *Staphylococcus aureus* lasted 48 hours. The conditions A, B, C and D were also measured and shown in Figure 40. Condition A is presented by graph a). Condition B is illustrated by graph b) whereas Condition C by graph c). Moreover, graphs d), e), and f) represent respectively the optical measurements of the eight dilutions, 10^1 CFU, 10^2 CFU, 10^3 CFU, 10^4 CFU, 10^5 CFU,10^6 CFU, 10^7 CFU, 10^8 CFU (Condition D), the calibration line and the number of cell detached from the samples C-CDHA, F-CDHA and β-TCP.

As before, the sedimentation period was effective and prevented the influence of detached crystals. On the other hand, graph a) allowed a differentiation of the bacterial growths according to the materials. The curve relating to the β-TCP material had the log phase first then followed by the curves specific to C-CDHA and F-CDHA materials. This allowed to affirm that the number of bacteria adhered to the surface of the β-TCP is higher than the others.

The influence of each material on bacterial growth was also highlighted by comparing graphs a) and b). Indeed, on graph b), the curves were identical for each material. This proved that it is not the detached crystals of the materials that act on the bacteria but the different topographies themselves as presented in graph a). The detached crystals have once again no influence on the bacteria as illustrated on graph c).

Furthermore, the representation of growth curves for the different known bacterial concentrations in graph d), allowed to draw the calibration curve corresponding to an optimal density of 0,5, graph e). By selecting the time value corresponding to the O.D. of 0.5 on graph a) for the C-CDHA, F-CDHA and β-TCP curves and by putting this value on the calibration curve, it was possible to determine the bacterial concentrations (CFU) specific to each material. As expected from the results of graph a), the β-TCP presents a higher concentration around $3,5.10^7$ CFU whereas the concentrations of the C-CDHA and the F-CDHA are close on 1.10^7 CFU.

Unfortunately, despite the success of bacterial count by this method the efficiency of SA detachment by 30 seconds of vortex was not enough on samples incubated for 48 hours. This was confirmed by confocal analysis of the samples that underwent 30 seconds of vortex. After the 48 hours of culture, SA might have develop an extracellular matrix more adherent on the surface of the samples that makes SA detachment difficult. A more intensive vortex or other routes for SA detachment should be investigated to improve the detachment efficiency.

a) Detached SA

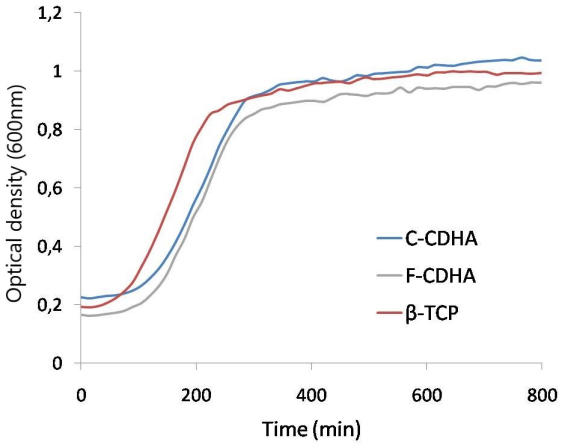

d) Bacterial growth curves

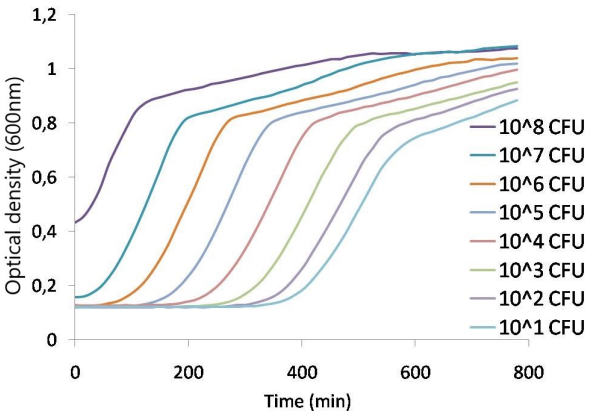

b) Control of crystal + SA

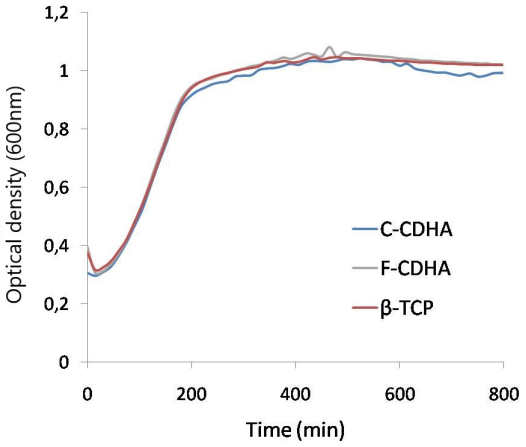

e) Calibration curve

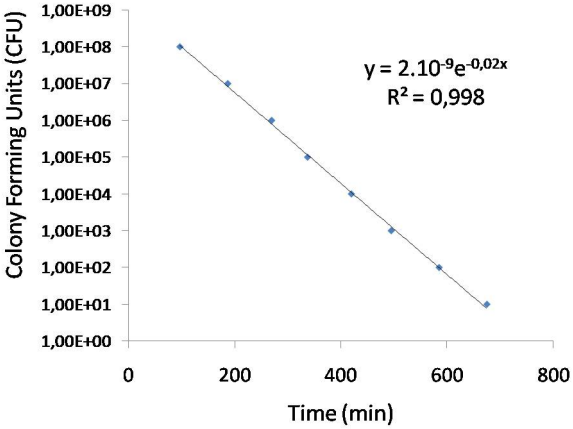

c) SA

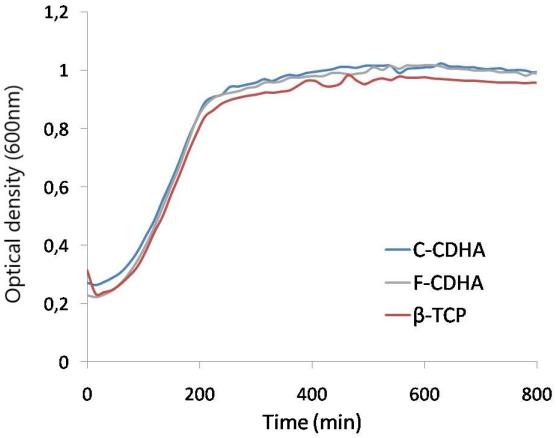

f) Number of cell detached from the samples

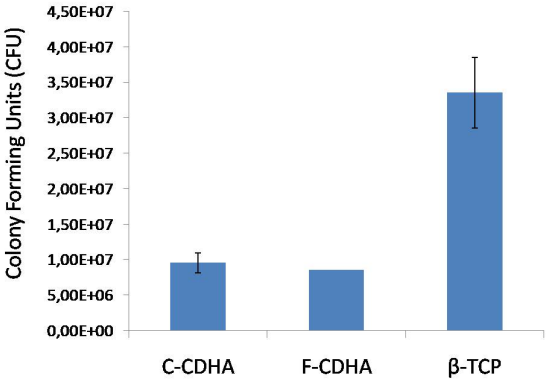

Figure 40: Optical density measurements after a *Staphylococcus aureus* adhesion and proliferation test of 48 hours on C-CDHA (blue), F-CDHA (grey) and β-TCP (red). Bacteria detachment: 30 seconds; a) detached SA; b) Control of crystal + SA; c) SA; d) Bacterial growth curves; e) Calibration curve; f) Number of cells detached from the samples.

5 Environmental impact analysis and safety measures

Throughout the project, environmental and safety precautions have been taken to reduce the environmental impact and the potential risks. The cleaning of the equipment and the waste management were particularly taken into consideration. In fact, they have a very important environmental influence. Depending on the toxicity or dangerousness of the handled products, end-of-life precautions must be observed. Safety precautions must of course also be taken into account.

Few products with risks for the users were handled. Nevertheless, each manipulation was performed by being equipped with a blouse and gloves to avoid contact with the skin. Closed shoes wee also required in case of falling products. Only Live/Dead dye and glutaraldhehyde present significant risks. Indeed, Live/Dead dye is mutagenic and glutaraldehyde is corrosive and toxic. The recovered waste containing these two products was treated with particular attention and separated from harmless products. Indeed, the laboratory provided containers specific for each family of products.

Finally bacteria manipulations must be controlled and isolated from other manipulations to avoid any risk of contamination. The bacteria *Staphylococcus aureus* used in the manipulations belonged to the lowest safety level, they can be consequently handled in the BBT laboratories of PC1 biosafety level. The manipulations were therefore performed in a sterile hood and the material used was sterilized or cleaned with ethanol before use. On the other hand, the material that was in contact with the bacteria must be separately thrown from the other waste. A special garbage bin was provided for these garbage only, regardless of the type of materials (paper, plastic or liquids). When the bin was full, the contents were sterilized by autoclaving and then considered as a conventional waste.

6 Conclusions

The present project had successfully confirmed that CaP biomaterials with similar chemistry but different topographies have the ability to alter bacterial attachment and growth in the following order: F-CDHA $<$ C-CDHA $\leq$ Fc-CDHA $=$ β-TCP.

The most clear trend was however for the F-CDHA which showed the lowest proliferation among materials. Evaluation of the percentage of SA surface coverage gave half the value compared to the rest of the materials after 48 hours of incubation. This results put forward the ability of nanostructured needle-like crystals to help delaying bacteria proliferation.

In regards to the quantification of SA on the different materials, two different methods have been compared: a semiqualitative method based on the fluorescence of attached SA and a quantitative method based on SA detachment. The former allowed a quick screening of SA surface coverage but unfortunately the results only allowed measuring SA projected in the 2D image. Bacteria growing in multilayers were not considered. The later instead, was more time consuming but could provide data of the whole sample. Despite the promising results of this later approach, further studies are required to improve the detaching efficiency of *Staphyloccocus aureus* at longer incubation times.

7 Economic analysis

The economic analysis deals with the different costs generated during the project. The costs related to the products are summarized in Table 8. The costs related to equiments are presented in Table 9. The costs due to personnel interventions are collected in Table 10. Finally, Table 11 discloses the cost total project.

Products	Quantity	Price	Cost (€)
24-well plate	40 plates	65€/5plates	520
96-well plate	4 plates	200€/5plates	160
Calcium carbonate ($CaCO_3$)	96,798 g	180€/500g	35
Calcium phosphate dibasic ($CaHPO_4$)	263,178 g	25€/100g	66
Absolute ethanol	200 mL	0,03 €/mL	6
BHI media	37 g	37,95€/100g	14,04
Distilled Water	4 L	15€/25L	2,4
Falcon 15mL	50 units	200€/500 units	20
Falcon 50mL	35 units	150€/500 units	10,5
Gloves S size	1 boxe	5€/boxes	5
Live/Dead dye	1/3 kit	640/kit	213,34
Pasteur pipette 3mL	5 units	23,30€/500 units	0,2
PBS 10x	5 discs	168€/100 discs	8,4
Precipitated Hydroxyapatite	3 g	24,6€/g	73,8
SEM pin	40 units	160€/800 units	3
Staphylococcus aureus strain	1/10 strains	50 €/strain	5
Sterile 10 mL glass pipette	10 units	33,50 €/200 units	1,7
Tips 1mL	300 units	54,17€/960 units	17
Tips 200	50 units	59,28€/960 units	3,09
Total cost of the products			1164,47

Table 8: Analysis of the costs related to the products used during the project

Equipment	Used time (h)	Price (€/h)	Cost (€)
Autoclave	2	30	60
Carbon deposition for SEM sample preparation	1	30	30
Microplate reader	60	20	1200
Flow hood	150	20	300
Fluorescent confocal microscope	30	30	900
Furnace	30	8	240
Planetary mill	6	6	36
SEM	18	40	720
Speedmixer	0,5	3	1,5
XRD	2	36,41	72,82
Total cost of equipment (€)			3560,32

Table 9: Analysis of the costs related to the equipment used during the project

Personnel intervention	Worked hours (h)	Salary (€/h)	Cost (€)
Post-doctoral researcher (co-director)	80	42	3360
Technical Team	35	30	1050
Master student	600	0	0
Total cost of personnel intervention (€)			4710

Table 10: Analysis of the costs related to the personnel intervention during the project

Total cost of the products (€)	1164,47
Total cost of the equipment (€)	3560,32
Total cost of the personnel interventions (€)	4710
Total cost of the project (€)	9434,79

Table 11: Analysis of the total cost of the project

8 References

[1] S. V Dorozhkin and M. Epple. Biological and medical significance of calcium phosphates. Angew. Chemie Int, vol.41, no. 17, pp. 3130-3146, 2002.

[2] Jill D. Pasteris, Brigitte Wopenka and Eugenia Valsami-Jones. Bone and Tooth mineralization: why apatite?. Vol.4, no. 2, p. 97-104. 2008.

[3] Sadat-Shojai, M. and al., Acta Biomater., 9, 7591. 2013.

[4] Maria-Pau Ginebra, Montserrat Espanol, Yassine Maazouz, Victor Bergez and David Pastorino. Bioceramics and bone healing. Efort Open Rev, vol.3. 2018.

[5] M. Bohner. Calcium orthophosphates in medicine: from ceramics to calcium phosphate cements. Injury, 31, D37–D47.2000.

[6] S. Dorozhkin. Biceramics of calcium orthophosphates. Biomaterials, vol.31, no. 7. pp. 1465-85. 2010.

[7] R.Gunzburg, M. Szpalski, N. Passuti and M. Aebi. The Use of Bone Substitutes in Spine Surgery. 2001.

[8] R.G. Carrodeguas and S. De Aza. α tricalcium phosphate : synthesis, properties and biomedial applications. Acta Biomater., 7, 3536-3546. 2011.

[9] E. R. Kreidler and F. A. Hummel. Phase relations in the system SrO-P2O5 and the influence of water vapor on the formation of Sr4P2O9. Inorganic Chemistry, 6(5), 884–891. 1967.

[10] J. H. Welch and W. Gutt. High-Temperature Studies of the System Calcium Oxide–Phosphorus Pentoxide. J. Chem. Soc., 4442–4. 1961.

[11] G. Trömel, H. J. Harkortz and W. Hotop. Untersuchungen im System CaO–P2O5–SiO2. Z. Anorg. Chem., 256 [5–6] 253–72. 1948.

[12] I. Barin. Thermochemical Data of Pure Substances, Part I—II. VCH Verlags Gesellschaft, Weinheim. 1993.

[13] HSC Outokumpu. Chemistry for Windows. v 5.1, Outokumpu Research Oy Information Service. 2002.

[14] W. M. Chase. NIST-JANAF Thermochemical Tables/Malcolm. National Institute of Standards and Technology, 4th edition, Edited by W. Chase Jr. The American Institute of Physics/The American Chemical Society Cop.. 1998.

[15] B. Dickens, L. W. Schroeder and W. E. Brown. Crystallographic Studies of the Role of Mg as a Stabilizing Impurity in b-Ca3(PO4)2. The Crystal Structure of Pure b-Ca3(PO4)2. J. Solid State Chem., 10 [3], 232–48. 1974.

[16] M. Yashima and A. Sakai. High-Temperature Neutron Powder Diffraction Study of the Structural Phase Transition Between a and a0 Phases in Tricalcium Phosphate Ca3(PO4)2. Chem. Phys. Lett., 372, 779–83. 2003.

[17] M. Mathew, L. W. Schroeder, B. Dickens and W. E. Brown. Crystal Structure of Alpha-Ca3(PO4)2. Acta Crystallogr., B33 [5] 1325–33. 1977.

[18] M.P. Ginebraa, M. Espanol, E.B. Montufara, R.A. Pereza and G. Mestresa. New processing approaches in calcium phosphate cements and their applications in regenerative medicine. Acta Biomaterialia, 6, 2863–2873. 2010.

[19] Ginebra MP. Calcium phosphate bone cements. In: Deb S, editor. Orthopaedic bone cements. Cambridge: Woodhead Publishing Limited, 206–30. 2008.

[20]Lewis G. Injectable bone cements for use in vertebroplasty and kyphoplasty: state-of-the-art review. J Biomed Mater Res B, 76:456–68. 2006.

[21] A. M. Rogues. UE 2.10. Infectiologie-Hygène, Agents infectieux. 2015.

[22] Bacteria drawing rod shaped [Online]. Available: https://ubisafe.org/explore/bacteria-drawing-rod-shaped/

[23] Diagramm of Gram Positive and Gram Negative Bacteria cell wall [online]. Available: https://thatspa.co/optional-diagram-of-gram-positive-and-gram-negative-bacteria-cell-wall.php

[24] S. N. Taylor, R. P. DiCarlo and D. H. Martin. Comparison of methylene blue/gentian violet stain to Gram's stain for the rapid diagnosis of gonococcal urethritis in men. 38(11):995-6. 2011.

[25] Gram Staining: Principle, Procedure and Results [Online]. Available: https://microbeonline.com/gram-staining-principle-procedure-results/

[26] What are the differences between Gram-positive and Gram-negative bacteria? [Online]. Available: https://www.quora.com/What-are-the-differences-between-Gram-positive-and-Gram-negative-bacteria

[27] Samantha E. McBirney, Kristy Trinh, Annie Wong-Beringer and Andrea M. Armani. Wavelength-normalized spectroscopic analysis of *Staphylococcus aureus* and *Pseudomonas aeruginosa* growth rates. 7(10): 4034–4042. 2016.

[28] Okada M, and al. Structure of the Bacillus subtilis quorum-sensing peptide pheromone ComX. Nat Chem Biol. 1: 23-24. 2005.

[29] Muhsin Jamal, Ufaq Tasneem, Tahir Hussain and Saadia Andleeb. Bacterial Biofilm: Its Composition, Formation and Role in Human Infections. Research Reviews. 2015.

[30] Costerton J, and al. Bacterial biofilms: a common cause of persistent infections. Sci. 284: 1318-1322. 1999.

[31] Mckenney D, and al. The ica locus of Staphylococcus epidermidis encodes production of the capsular polysaccharide/adhesin. Infect Immunity. 66: 4711-4720. 1998.

[32] L. Hall-Stoodley, J. W. Costerton and P. Stoodley. Bacterial biofilms: from the natural environment to infectious diseases. 2(2):95-108. 2004.

[33] Spellberg, B., Blaser, M., Guidos, R., Boucher, H., Bradley, J. and al.. Infectious Diseases Society of America. Combating antimicrobial resistance: policy recommendations to save lives. Clin Infect Dis 52(Suppl. 5): S397–S428. 2011.

[34] H. Goossens, M. Ferech, R.Vander Stichele, M. Elseviers and ESAC Project Group. Outpatient antibiotic use in Europe and association with resistance: A cross-national database study. Lancet 365: 579–587. 2005.

[35] C. Llor and L. Bjerrum. Antimicrobial resistance: risk associated with antibiotic overuse and initiatives to reduce the problem. Therapeutic Advances in Drug Safety, 5(6), 229–241. 2014.

[36] Andie S. Lee, Hermínia de Lencastre, Javier Garau, Jan Kluytmans, Surbhi Malhotra-Kumar, Andreas Peschel and Stephan Harbarth. Methicillin-resistant *Staphylococcus aureus*. Nature Reviews Disease Primers. 2018.

[37] Jelmer Sjollena, Sebastian A.J. Zaat, Veronique Fontaine, Madeleine Ramstedt, reto Luginbuehl, Karin Thevissen, Jiuyi Li, Henny C. van der Mei and Henk J. Busscher. In vitro methods for the evaluation of antimicrobial surface designs. Acta Biomater. 12-24. 2018.

[38] M. Cloutier, D. Mantovani and F.Rosei. Antibacterial Coatings: Challenges, Perspectives, and Opportunities. Trends in Biotechnology, 33(11), 637–652. 2015.

[39] H. Özçelik, N. E. Vrana, A. Gudima, V. Riabov, A. Gratchev, Y.Haikel and P. Lavalle. Harnessing the Multifunctionality in Nature: A Bioactive Agent Release System with Self-Antimicrobial and Immunomodulatory Properties. Advanced Healthcare Materials, 4(13), 2026–2036. 2015.

[40] J. C.Tiller, Designing surfaces that kill bacteria on contact. Proc. Natl. Acad. Sci. U.S.A. 98, 5981–5985. 2001.

[41] K. Lewis and A. M. Klibanov. Surpassing nature: rational design of sterile surface materials. Trends Biotechnol. 23, 343–348. 2005.

[42] J-B.D Green. A review of immobilized antimicrobial agents and methods for testing. Biointerphases 6, MR13–MR28. 2011.

[43] Marieke van de Lagemaat, Arjen Grotenhuis, betsy van de belt-Gritter, Steven Roest, Ton J.A. Loontjens, henk J.Busscher, Henny C. Van der Mei and Yijin Ren. Comparison of methods to evaluate bacterial contact-killing materials. Acta Biomater.. 139-147.2017.

[44] J. Hasan. Antibacterial surfaces: the quest for a new generation of biomaterials. Trends Biotechnol. 31, 295–304. 2013.

[45] R. S. Friedlander ; Bacterial flagella explore microscale hummocks and hollows to increase adhesion. Proc. Natl. Acad. Sci. U.S.A. 110, 5624–5629. 2013.

[46] F. Variola. Oxidative nanopatterning of titanium generates mesoporous surfaces with antimicrobial properties. Int. J. Nanomed. 9, 2319–2325. 2014.

[47] J. Meng, P. Zhang and S. Wang. Recent Progress in Biointerfaces with Controlled Bacterial Adhesion by Using Chemical and Physical Methods. Chemistry - An Asian Journal, 9(8), 2004–2016. 2014.

[48] E. P. Ivanova, J. Hasan, H. K. Webb, V. K. Truong, G. S. Watson, J. A. Watson, V. A. Baulin, S. Pogodin, J. Y. Wang, M. J. Tobin, C. Lçbbe and R. J. Crawford. Natural Bactericidal Surfaces: Mechanical Rupture of Pseudomonas aeruginosa Cells by Cicada Wings. Small. 8, 2489 – 2494. 2012.

[49] A. I. Hochbaum, J. Aizenberg and Nano Lett. Bacteria Pattern Spontaneously on Periodic Nanostructure Arrays. 10, 3717 – 3721. 2010.

[50] Kenneth K. Chung, James F. Schumacher, Edith M. Sampson, Robert A. Burne, Patrick J. Antonelli, and Anthony B. Brennan. Impact of engineered surface microtopography on biofilm formation of *Staphylococcus aureus*. Biointerphases 2, 89. 2007.

[51] A. N. Naimushin, S. D. Soelberg, D. K. Nguyen, L. Dunlap, D. Bartholomew, J. Elkind and C. E Furlong. Detection of *Staphylococcus aureus* enterotoxin B at femtomolar levels with a miniature integrated two-channel surface plasmon resonance (SPR) sensor. Biosensors and Bioelectronics, 17(6-7), 573–584. 2002.

[52] S. Balasubramanian, I. B. Sorokulova, V. J. Vodyanoy and A. L. Simonian. Lytic phage as a specific and selective probe for detection of *Staphylococcus aureus*—A surface plasmon resonance spectroscopic study. Biosensors and Bioelectronics, 22(6), 948–955. 2007.